Biophysical Journal
Biophysical perspective

Biophysical Society

The molecular mechanism of ATP synthase constrains the evolutionary landscape of chemiosmosis

J. Emyr Macdonald[1,*] and Paul D. Ashby[2]
[1]School of Physics and Astronomy, Cardiff University, The Parade, Cardiff CF24 3AA, UK and [2]Molecular Foundry, Lawrence Berkeley National Laboratory, Berkeley, CA 94720

ABSTRACT ATP synthase, the enzyme responsible for regenerating adenosine triphosphate (ATP) in the cell, comprises a proton-translocating motor in the cell membrane (labeled F_O in bacteria, mitochondria, and chloroplasts), coupled by a common stalk to a catalytic motor F_1 that synthesizes or hydrolyzes ATP, depending on the direction of rotation. The detailed mechanisms of F_O, F_1 and their coupling in ATP synthase have been elucidated through structural studies, single-molecule experiments, and molecular modeling. The outcomes of this body of work are reviewed with a particular focus on the features of the mechanism that enable the high energy efficiency and reversibility of ATP synthase. Models for the origin of chemiosmosis involve either ATP synthesis (driven by the proton gradient across the membrane) or ATP hydrolysis (for pumping protons out of the cell) as a primary function, the other function being a later development enabled by the coupled nature of the two motors. The mechanism of ATP synthase and the stringent requirements on efficiency to maintain life constrain existing models and the search for the origin of chemiosmosis.

SIGNIFICANCE ATP synthase is the enzyme primarily responsible for synthesizing adenosine triphosphate (ATP) in the cell. It consists of a proton-driven motor, labeled F_O, coupled by a common shaft, to a chemical motor F_1 that synthesizes or hydrolyzes ATP, depending on the direction of rotation. The detailed understanding of the mechanisms of ATP synthase that has emerged from structural studies, nanoscience, and molecular modeling is reviewed. The mechanism leads to discussion of constraints on the evolutionary landscape that gave rise to chemiosmosis.

INTRODUCTION

Hydrolysis of adenosine triphosphate (ATP) is central to biological energy conversion in the cell. This most common of enzymatic reactions enables essential thermodynamically uphill processes. The free energy is available as a result of the cell's maintenance of the ratio of concentrations $[ATP]/[ADP][P_i]$ well away from equilibrium by about nine orders of magnitude. Continual regeneration of ATP from the hydrolysis products, adenosine diphosphate (ADP) and a phosphate ion (P_i), is therefore vital for any living cell to prevent rapid and lethal drift toward equilibrium. Despite its high free energy of hydrolysis of around 50 kJ mol^{-1} (20 k_BT) under cellular conditions, ATP is remarkably stable in solution, having a half-life of around a year, the activation energy for its hydrolysis being around 140 kJ mol^{-1} (1,2). This high degree of stability relates to the difficulty in maintaining proximity and orientation of water molecules for effective nucleophilic attack on the phosphorus orbitals. In this way, dissipation of Gibbs free energy by hydrolysis of ATP is prevented except when bound to specific enzymes. Enzymes that hydrolyze ATP in order to perform work or to drive endergonic reactions are referred to as ATPases. ATP synthase is the ubiquitous enzyme that is responsible for the regenerative synthesis of ATP from the hydrolysis products ADP and P_i.

The ATP synthase enzyme comprises a membrane-bound electrochemical motor coupled to a catalytic chemical motor by a common stalk (3–6). In bacteria, mitochondria, and chloroplasts, these motors are labeled F_O and F_1 respectively. The F_O motor comprises the *a*-subunit and a rotor ring c_n of *n* identical subunits where *n* varies between eight and 17 depending on species (3). The two motors are held together by the rotating central stalk and the static

Submitted November 14, 2024, and accepted for publication May 15, 2025.
*Correspondence: macdonald@cardiff.ac.uk
Editor: Sua Myong.
https://doi.org/10.1016/j.bpj.2025.05.017

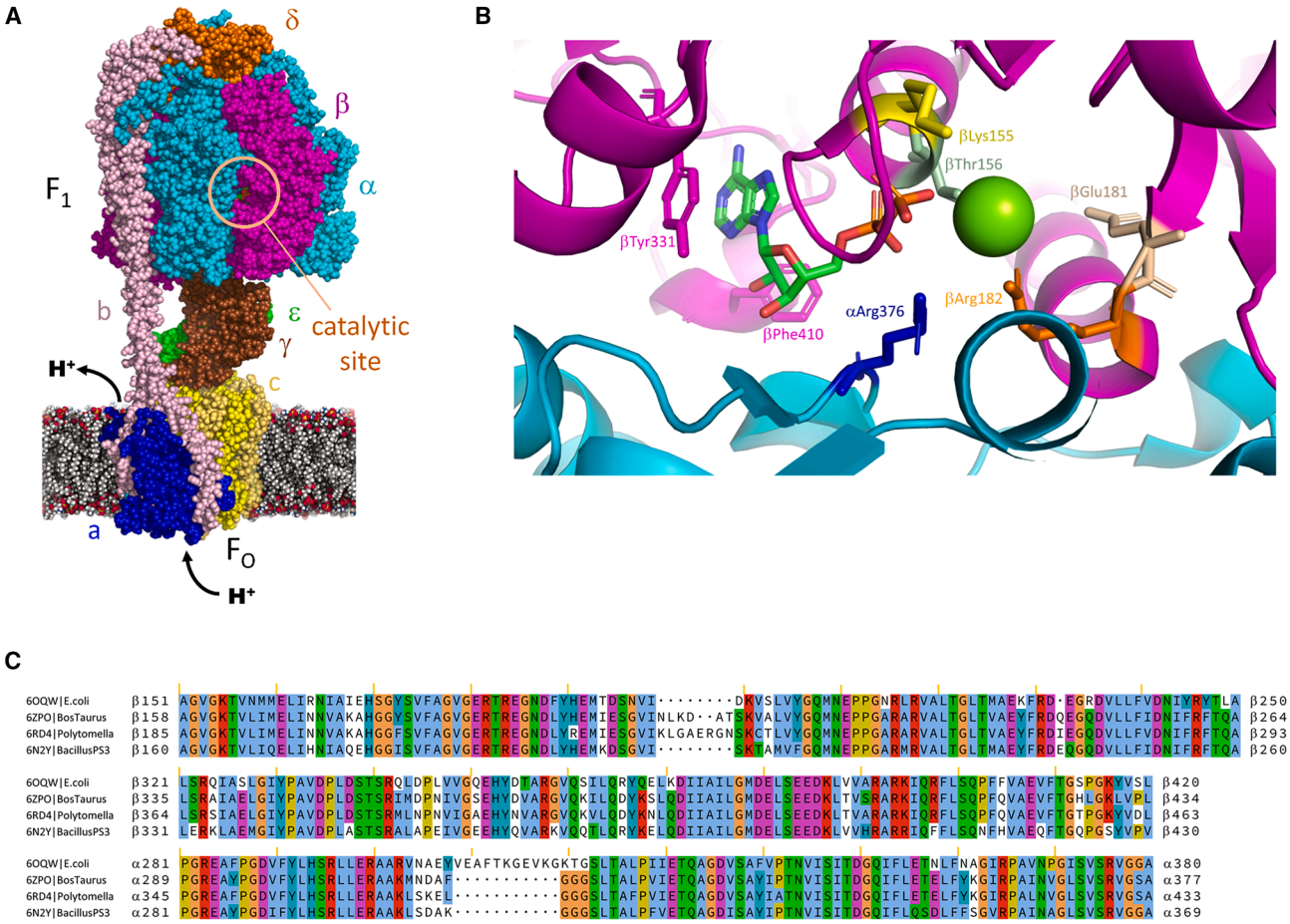

FIGURE 1 (*A*) The molecular structure of F_O-F_1 ATP synthase from *E. coli* (PDB: 8dbq) determined from cryo-electron microscopy (7). Its subunits are α (*cyan*), β (*magenta*), γ (*brown*), δ (*orange*), ε (*green*), a (*blue*), b (*pink*), and c (*yellow*). (*B*) The active catalytic site in the β_{DP} subunit (*shown in magenta*) at its interface with the α-subunit (*in cyan*). Colored side chains denote some of the crucial residues that are mentioned in the text. Aromatic side chains colored magenta denote those that interact with the adenine ring. The nucleotide is ADP: the Pi is absent in the cryo-electron microscopy structure although a Mg^{+2} ion (*green sphere*) is included. (*C*) A multiple sequence alignment for the β subunit catalytic site and α subunit at the interface with the β subunit from different organisms to facilitate comparison. Residues are colored according to the Clustalx scheme (*blue: hydrophobic, red: positively charged, magenta: negatively charged, green: polar, cyan: aromatic, pink: cysteines, orange: glycines, dark yellow: prolines*). Vertical wheat-colored bars denote multiples of ten in the residue index of *E. coli*.

peripheral stalk, which connect the respective rotors and stators. The full structure of the F_OF_1 ATP synthase of *E. coli*, determined using cryo-electron microscopy (cryo-EM), is shown in Fig. 1 *A* (7). The ATP synthase complex can operate reversibly with extremely high efficiency in two different modes, depending on the relative torque generated by the two motors. If the F_1 motor generates the greater torque by hydrolysis of ATP, then it turns the central stalk in the anticlockwise direction, as the F_1 motor is viewed from the membrane, and F_O is driven in reverse to pump protons out of the cell. Conversely, if the torque of the F_O motor generated by proton flow dominates, the central rotor shaft turns in the opposite direction, driving the F_1 motor in reverse to synthesize ATP from ADP and P_i. In common with other molecular motors, steps are stochastic in nature at the single-molecule level with forward and reverse steps being observed in a viscous aqueous environment dominated by Brownian fluctuations (8–12). In mitochondria and chloroplasts, in vivo, ATP synthase only acts to synthesize ATP, whereas in bacteria, the enzyme will either hydrolyze or synthesize ATP depending on growth conditions (3).

All proposed models for the origin of chemiosmosis inevitably involve the evolution of either proton pumping or ATP synthesis as a primary function, the other function being a later development enabled by the coupled nature of the two motors. Models in which the proposed initial function was to pump protons out of the cell (13), powered by ATP generated by an alternative mechanism usually assumed to be fermentative, will be referred to as ***Hydrolysis-First***, whereas those involving the early emergence of chemiosmosis for synthesis of ATP will be labeled ***Synthesis-First***. In the 1970s and 1980s, the common view was that the earliest metabolic pathways for generating ATP involved substrate-level phosphorylation in fermentation reactions

(13–15). Substrate-level phosphorylation in solution does not require compartmentation by membranes, does not involve electron flow, and can occur under anaerobic conditions before the appearance of photosynthesis, consistent with conditions on the early earth. Raven and Smith (13) presented a coherent sequence of events leading from fermentation to chemiosmosis, which formed the basis of textbook treatments (16). This Hydrolysis-First viewpoint was later challenged. Lane and co-workers noted that the low net Gibbs free energy released by glycolysis requires sophisticated and energetically efficient metabolic cycles: around 12 enzymes are required in the sequence of steps in current glycolytic fermentation. Enzymes and molecular complexes that consumed the ATP thus generated would also need to be highly efficient to harness the low available free energy. Secondly, they noted that bacteria and archaea employ enzymes having significantly different amino acid sequences and fold conformations to catalyze individual steps of fermentation, whereas the hydrolytic catalytic sites of the ATP synthase in bacteria and archaea are homologous (F_1 and A_1 subunits respectively), though their central and peripheral stalks differ. If traits shared by archaea and bacteria are inherited from a common ancestor, then ATP synthase, in common with the ribosome, is likely to predate the last universal common ancestor (LUCA), whereas fermentation is likely to have appeared later (17,18).

The requirement for primitive life to be maintained well away from equilibrium led to increased interest in hydrothermal vent systems as locations for transition from an abiotic proto-metabolism involving inorganic catalysts to early metabolic cycles enabled by enzymes. In contrast to the open ocean, where there is no obvious source of free energy to drive energetically uphill reactions, vents provide local gradients of chemical/redox potential and pH. Their microporous structure could provide for compartmentation and local concentration of organic molecules (19). Popular proposed scenarios include deep-sea (20) or shallow-sea (21) alkaline hydrothermal vents as locations for autotrophic early life, driven by an inexhaustible supply of geothermal energy to synthesize more complex molecules (17). To date, substantive proposals for bridging of the gulf between prebiotic inorganic origins and the elegant and energetically efficient ATP synthase molecular machine are currently absent for this Synthesis-First scenario.

Over the last three decades, the detailed mechanisms of ATP synthase continue to be elucidated through structural studies, single-molecule experiments, and molecular modeling. Advances in cryo-EM have led to dynamical models of the full complex, building on the important earlier results of synchrotron-based x-ray diffraction in determining the structure of crystallized portions of the enzyme (22–27). Single-molecule experiments have enabled nanoscale forces to be measured, individual steps in sequential processes to be visualized, and kinetics determined. Since all current cellular life shares a chemiosmotic complex that regenerates ATP rapidly after it is consumed by hydrolysis, any postulated stage in the evolution of chemiosmosis should have a relatively continuous path backward to prebiotic origins on the early earth and forward to modern organisms (28). Whereas the early stages of such a path are difficult to probe, the later transitional stages must relate directly to current mechanisms. Here, we summarize the current understanding of the mechanism of the ATP synthase complex and find that the required efficiency needed for ATP synthase to sustain a physiologically viable concentration ratio, [ATP]/[ADP], in the cell is an exacting constraint, which should guide future hypotheses for ATP synthase evolution.

KEY ELEMENTS IN THE MECHANISM OF ATP SYNTHASE

Coordinated motion in ATP synthase arises from effective coupling of catalysis in the F_1 subunit to the free energy change of protons as they traverse the membrane through the F_O subunit. By the early 1990s, it had been inferred that the energy input from proton translocation in ATP synthesis mainly drives changes in binding of nucleotides at the catalytic sites of F_1 by conformational coupling, referred to as the binding change mechanism (29,30). The determination of the full crystallographic structure of the F_1 subunit by Walker and coworkers in 1994 (31,32) was crucial in establishing the basic molecular mechanism by which ATP synthase couples chemical energy of hydrolysis to mechanical rotation. This ground-breaking work established the overall structure of F_1 including the details of the catalytic site in the β-subunit at its interface with the neighboring α-subunit within the $(\alpha\beta)_3$ hexamer. The three β-subunits were shown to be in different conformations, in agreement with Boyer's binding change mechanism, one binding ATP, another binding ADP, and the third not having a bound nucleotide. Interactions were determined between the β-subunit and the γ-subunit of the central stalk, whose rotation drives these conformational changes. This crystallographic structure underpinned the progress made over the following two decades in the understanding of the mechanism of ATP synthase.

The motor's rotary motion was elegantly demonstrated by a pioneering single molecule experiment in which the rotation of the F_1 motor was directly visualized (33). This study led to a series of innovative nanoscale single-molecule experiments that detailed the sequence of events, dynamics, catalytic site occupancies (9), chemical affinities (34), angular velocities (35), and mechanical torque (36,37) as a function of rotation angle γ. These developments, in parallel with further crystallographic structure determinations, quantum mechanical molecular modeling (QM/MM) (38,39), and coarse-grained simulations (40), led to a detailed picture of the rotation cycle of F_1. The atomic structure of F_O was hampered for years by the difficulty in

crystallizing membrane proteins, but rapid technical improvements in cryo-EM led to detailed models of its mechanism (5,23,26,41). Before these developments, most experimental studies focused initially on the isolated F_1 motor, whose proteins are soluble in water, driven by ATP hydrolysis. The reversible nature and high efficiency of synthesis and hydrolysis in ATP synthase has enabled progress to be made in the mechanism of ATP synthesis based on results for the hydrolysis cycle. Cryo-EM and other approaches have more recently enabled ATP synthesis to be probed directly.

In the following subsections, we outline the detailed mechanisms of both F_1 and F_O arising from this body of work, together with the way they are coupled and regulated. It should be noted that the corresponding A_1 and A_O motors in archaea and in some extremophile bacteria along with V_1 and V_0 in the organelles of eukaryotes share structurally and sequentially homologous hexameric subunits. The structure of the central and peripheral stalks differs between bacterial and archaeal motors, whereas the essential mechanisms of catalysis and torque generation are shared. The analysis presented here is not significantly affected by the question whether early organisms were bacterial or archaeal in nature (17). For simplicity, we refer to F_1 and F_O motors throughout, without discounting possible archaeal origins. In section summary of the mechanism of F-type ATP synthase, we give a brief summary of essential parts of the mechanism for a general reader, less interested in the details, to lead into the discussion.

F_1 motor mechanism for ATP hydrolysis

The rotation cycle of the F_1 motor

The molecular structure of the catalytic site of F_1 is shown in Fig. 1 *B*. Each of the three catalytic sites is located in each β-subunit at its interface with the corresponding α-subunit. The catalytic site structure is described in several papers (5,23,31,32,39,42). The adenine ring sits in a hydrophobic pocket on the β-subunit held by βTyr31 and βPhe410. The main side chains from the β-subunit that interact with the endmost two phosphates, P_β and P_γ, are βGlu161, βArg182 and βLys155 together with other residues from the highly conserved P-loop whose backbone amine groups form hydrogen bonds to the phosphates. (Residues are indexed for *E. coli* throughout for consistency. The corresponding residues for other organisms can be found in Fig. 1 *C*). A Mg^{2+} ion contributes to charge neutralization of the catalytic site, being bonded to both P_β and P_γ and to a basic βThr156 residue. A water molecule responsible for nucleophilic attack on P_γ and a second coordinated water molecule, which transfers protons during catalysis, are bound by βGlu181 and βArg182 (39,43). The polarized hydrogen bonds with the neighboring residues draw electronic charge from P_γ toward P_β such that the local net charge in the transition state is close to zero (39). The basic long sidechain from the α-subunit (the "arginine finger"), αArg376, is crucial for catalytic efficiency (38,44) such that subtle changes in α- to β-subunit interactions play a coordinating role in kinetics the catalytic step within the rotation cycle. The rotation rate of ATP synthase of ∼100–700 Hz, driven by ATP hydrolysis (45), in various organisms represents an enzymatic acceleration of nine or ten orders of magnitude. The free-energy change ΔG_{hyd} for hydrolysis of a single molecule of ATP is

$$\Delta G_{hyd} = \Delta G_0' + k_B T \ln\left(\frac{[\mathrm{ADP}][\mathrm{P_i}]}{[\mathrm{ATP}]}\right), \qquad (1)$$

where $\Delta G_0' = -50.6$ pN nm (1.0 pN nm = 0.602 kJ mol^{-1}) is the standard free energy change at pH 7 under physiological conditions (46). $\tau_1 = -3\Delta G_{hyd}/2\pi$ is the corresponding mean torque of the F_1 motor, assuming efficient conversion of chemical free energy to mechanical work (with $\Delta G_{hyd} < 0$, $\tau_1 > 0$). Experimental values of torque agree well with calculated values of τ_1 over a range of nucleotide concentrations (36,37). The rate of ATP synthesis for a single enzyme molecule is around 10 ATP molecules per second under physiological conditions, though it is capable of ∼300 ATP s^{-1} at high [ADP] and low [ATP] (47).

Fig. 2 *A* summarizes the sequential changes in occupancy of the catalytic site, the conformational state of the β-subunits, and the key events as a function of the γ-rotation angle in the hydrolysis cycle of the thermophilic bacterium *Bacillus* PS3, which has been used for most single-molecule studies. For low [ATP], short dwells are observed immediately before ATP binding events and at catalytic hydrolysis events. Each β-subunit follows the same sequence, displaced by 120° from its neighbor. Initial binding of ATP to the empty catalytic site of the β_E-subunit (shown in red) at an angle defined as $\gamma = 0°$ is driven largely by π-π stacking of the adenine ring with neighboring aromatic residues (6,48). This initial bonding step involves a twisting motion of the C-terminal domain of the β-subunit, to a part-closed β_{HC} conformation (6). After this initial binding event, the main contribution to the F_1 motor torque comes from sequential formation of hydrogen bonds to the phosphates, causing the C-terminal of the β-domain to close progressively around the nucleotide to the β_{TP} conformation. This closing motion engages and pushes the γ–stalk, whose profile is asymmetric and whose rotation is eccentric in the region of contact. Principal component analysis was performed by Okazaki and coworkers on atomic coordinates from published structures obtained by x-ray crystallography in order to identify the main conformational changes at play (49). By reducing the motion of many atoms into a few representative variables, the principal components are able to capture the closing motion of the β subunit (PC1) and the tightening of the interface between the β and α subunits

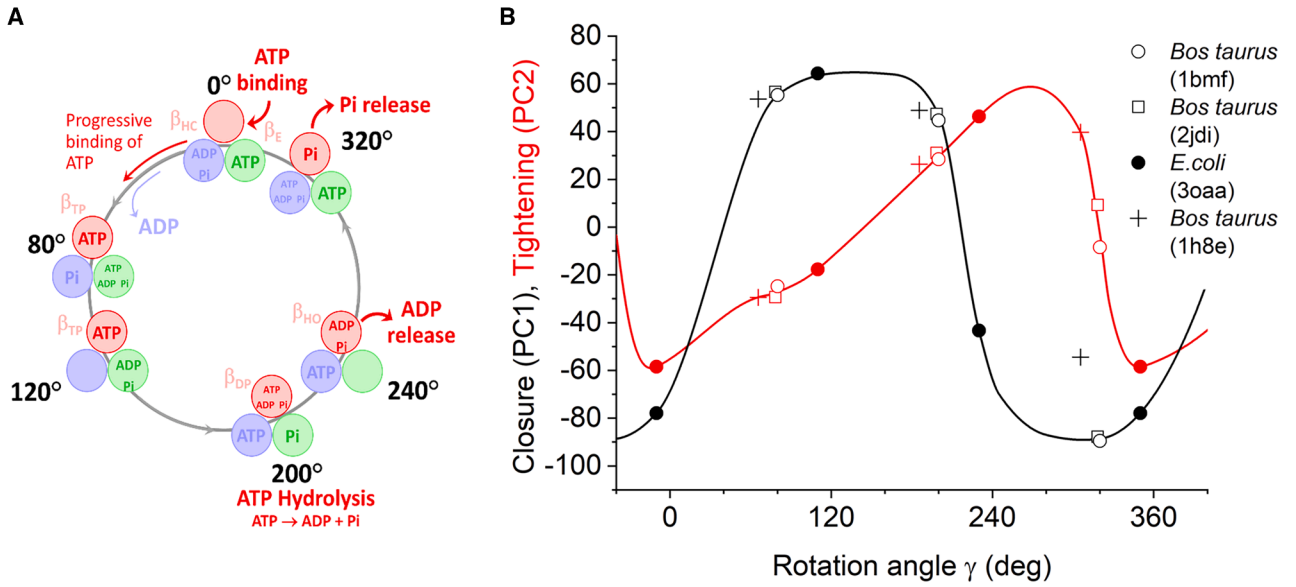

FIGURE 2 (*A*) Sequence of events in F_1 during the ATP hydrolysis cycle as a function of rotation angle γ from single-molecule experiments on the thermophilic bacterium *Bacillus* PS3 (adapted from [4]). $\gamma = 0°$ is the angle at which ATP initially binds to the empty catalytic site, colored red. Scission occurs at this site at $\gamma = 200°$, cleaving ATP into ADP and Pi. The two other binding sites of F_1 are offset by $\pm 120°$ and are shown in blue and green. (*B*) The principal components representing closure of the catalytic site (*black*) and tightening of the α-β interface (*red*) are shown as a function of γ for F_1. The key shows the PDB codes for the respective structures. The solid lines represent splines as guides to the eye.

(PC2). These are displayed as a function of rotation angle in Fig. 2 *B* (49,50). Although closure of the catalytic site accompanies ATP binding, subsequent tightening of the α-β interface is more gradual, the interface being most tight in the approximate range $\gamma = 200°$–$320°$. This tightening of the α-β interface pushes the arginine finger on the α-subunit, αArg376, into intimate contact with P_β and P_γ, thus stabilizing the planar, pentavalent transition state (51) for efficient catalysis. This insertion of the arginine finger is crucial for regulation of the rotation cycle, preventing ATP hydrolysis at rotation angles γ appreciably lower than 200° (44). After the catalytic scission of Pi at $\gamma \approx 200°$, ADP and P_i can be released sequentially at $\gamma \approx 240°$ and 320° respectively, where their affinities for the binding pocket are reduced (52). During rotation from $\gamma = 200°$ to $\gamma = 240°$, the β-subunit closes from the β_{DP} to the half-open β_{HO} conformation, with release of ADP occurring at or just after $\gamma = 240°$. During rotation from $\gamma = 240°$ to $\gamma = 320°$, an untwisting motion of the C-terminal domain of the β-subunit occurs, followed by release of Pi to restore the open β_E conformation (6), thus resetting the catalytic site to adsorb ATP for the subsequent cycle. Rotation cycles for F_1 motors from other organisms have been similarly characterized and show broadly similar behavior with minor differences in the γ angle at which events occur (45,53–57). The rotation cycles of archaeal and vacuolar ATP synthases have been less intensively studied (58–65), requiring further experimentation and molecular modeling to clarify the details of their mechanism. Subtle differences are observed between organisms. For example, for the V/A-ATPase from the thermophilic bacterium, *Thermus thermophilus*, single-molecule experiments reveal three pauses 120° apart (64). For *Enterococcus hirae*, initially observed to show three pauses 120° apart also (66), additional substeps were found (60), consistent with off-axis rotation of the rotor and stiff coupling between the V_O and V_1 subunits (63,65). Despite such differences, measurements of the angular velocity as a function of rotation angle showed almost identical profiles for both A_1 and F_1 motors, indicating broadly similar energy barriers during rotation (67).

Crucial factors for the high energy efficiency of F_1

The thermodynamic efficiency of the F_1 motor, measured by stalling against a conservative force, is very close to 100% (37). Its Stokes efficiency, measured for a rotating motor under viscous drag conditions, though less precisely determined, is approximately 90% (68). A helpful discussion of different measures of motor efficiency can be found in (69). Consideration of the stochastic thermodynamics of the coupled F_O-F_1 system, rather than the individual motors, leads to an overall efficiency of approximately 70–80% (70).

The high energy efficiency of F_1 is surprising when the relevant timescales are considered. ATP hydrolysis involves scission of its terminal phosphate group (P_γ), which, from the transition state, occurs rapidly on the fs-ps timescale. In contrast, the conformational changes that drive rotation of the central γ-stalk in ATP synthase occur on the μs-ms timescale, many orders of magnitude slower. If the free

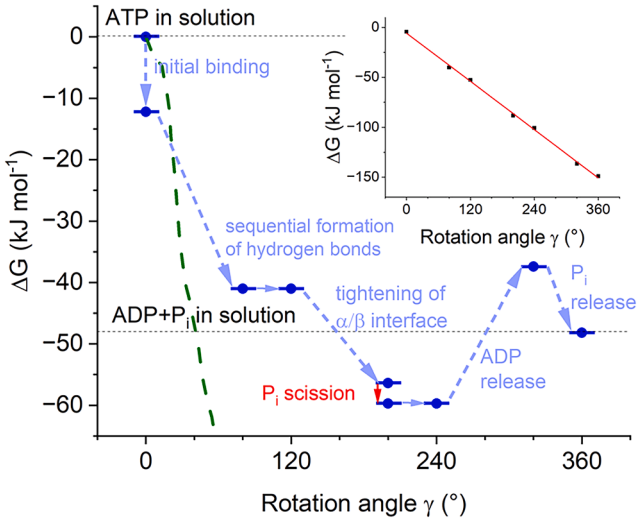

FIGURE 3 The approximate free energy landscape during hydrolysis of ATP within the catalytic site of the F_1 motor in ATP synthase as a function of rotation angle γ (adapted from (72)). Dashed pale-blue arrows represent processes that occur over slower μs–ms timescales and are coupled to conformational changes within the β- and α-subunits. The catalytic scission of the terminal phosphate of ATP, shown in red, is rapid (ps–fs timescale) and weakly exergonic. The free energy as a function of rotation angle calculated from molecular dynamics over the range $\gamma = 0°$–$60°$ (75) is shown by a dashed green line. The inset shows the free energy of three α-β subunit pairs, each offset by 120°, leading to an approximately constant torque.

energy of hydrolysis were released during the rapid scission of the terminal phosphate of the ATP molecule then the energy would be dissipated by relaxation processes as heat on the nanosecond timescale, long before the changes in conformation could occur (71,72). The sequence of events in the rotation cycle of ATP synthase described above is key to avoiding such complete thermal dissipation. The free energy is harnessed during *progressive binding of ATP* in the approximate range $\gamma \approx 0°$–$60°$. The significance of the progressive binding of ATP by sequential formation of hydrogen bonds now becomes apparent. As each hydrogen bond forms between P-loop residues of the catalytic site and the P_γ and P_β phosphate groups of ATP couple directly to rotation of the central γ-stalk (73) and the site's affinity for ATP increases, favoring the formation of the next hydrogen bond. In effect, this series of states having increasing affinity for ATP act as a succession of quasi-static states that are key to the motor's thermodynamic reversibility. In this way, harnessing of free energy occurs gradually to drive rotation, avoiding the thermal dissipation that inevitably results from rapid bond scission (72). As a result of this increasing affinity for ATP, the free energy decreases progressively with increasing angle, consistent with single-molecule experimental results (34,52). During this torque-generating sequence, it is important that the ATP molecule is kept intact with scission to ADP and P_i being suppressed until the introduction of the arginine finger into the catalytic site. QM/MM calculations confirm that the scission event is suppressed in the β_{TP} conformation before the insertion of the arginine finger into the catalytic site, whereas it becomes mildly exergonic ($\Delta G_{scission} \approx -3.3$ kJ mol^{-1}) in the β_{DP} conformation with the arginine finger introduced (38,39). The hydrolysis products, ADP and P_i, are released later in the cycle when their binding affinities are significantly lower (30,71).

A key target in advancing the understanding of F_1 and V_1 motors is a calculation of their free energy landscapes as a function of rotation angle and the modeling of their dynamics. Molecular dynamics and QM/MM simulations are hampered by the size of the system and the timescales of conformational changes and rotation. The approximate free energy landscape during the rotation cycle determined by Nam and Marcus from binding equilibrium data (72,74) is shown in Fig. 3. Such data do not provide precise numerical values for the operating motor, but they do give a qualitative picture. Also shown are calculated free energies over the range $\gamma = 0°$–$60°$ from molecular dynamics (75). These show the continual decrease in free energy in this angular range for ATP residing in the catalytic site, though the slope may be slightly inflated due to incomplete convergence (75). The corresponding calculations in the absence of ATP also reproduce the free energy minimum for the empty site (76). Coarse-grained simulations of the free energy for the rotation cycle (40,77) fail to reproduce the decrease in free energy in the range $\gamma = 0°$–$60°$ but give a continual increase of free energy in this region. Such an increase in free energy is inconsistent with single-molecule experiments and with the known energy cost of releasing ATP in the synthesis cycle (29). A prime target for future work should be the calculation of the free energy landscape for the full rotation cycle using all-atom molecular dynamics.

F_O motor mechanism

The F_O motor generates torque in the opposite direction to F_1 driven by protons (or Na^+ ions) diffusing into the cell along a specific channel around the c-ring. Whereas the key concepts for its mechanism were proposed almost three decades ago (78,79), a detailed description of the structure and mechanism of F_O became attainable recently with advances in the spatial resolution of cryo-EM (3). The rotary mechanism of F_O was determined for the unicellular alga *Polytomella* sp. (41) (Fig. 4), the same mechanism being also observed in chloroplasts (80), bacteria (22), and archaea (62). Here, we again index residues consistently with *E. coli*.

In driving ATP synthesis, protons enter the a-subunit of F_O from the low pH side of the membrane, along a half-channel lined by conserved polar residues to emerge at the a-c interface. Protons transfer sequentially via residues aAsp119, aGlu219, aAsn214, and aHis245 by a Grotthuss mechanism (5,26) onto the negatively charged carboxylate

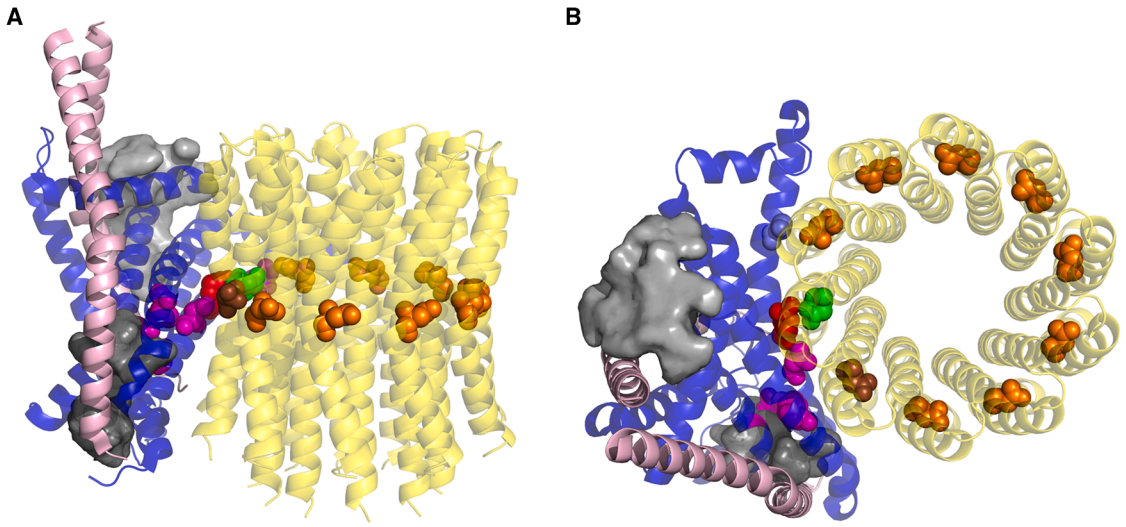

FIGURE 4 The F_O motor of *E. coli* (PDB: 6oqs) during ATP synthesis. Its subunits are a (*blue*), b (*pink*), and c (*yellow*). Residues cAsp61 which are protonated are shown in orange, with the most recently protonated being shown in a darker sienna color. The cAsp61 residue after releasing its proton to the pale gray outlet half-channel is shown in green. The direct path for protons between the two half-channels is electrostatically blocked by the aArg210 residue (*red*). The deprotonated cAsp61residue will be protonated by Grotthuss transfer of protons from the dark gray inlet half-channel, via residues shown in magenta, before it arrives at the sienna-colored site. The resulting biased rotation of the c-subunit is in the anticlockwise direction. (*A*) Side view. (*B*) Top view.

ligand (cAsp61) of the nearest unit of the c_n-ring, neutralizing its charge (Fig. 4). The exit half-channel is similar, laterally displaced along the a-c interface by $\sim$ 10 Å, the direct route between them being electrostatically blocked to protonated cAsp61 residues by an essential conserved arginine residue (aArg210 shown in red in Fig. 4) between entrance and exit half-channels (5,41). Their direct path from the entry half-channel to the exit half-channel being blocked by the conserved arginine, the protonated c-unit steps stochastically in the opposite direction. This brings a recently deprotonated cAsp61, shown in green in Fig. 4, close to aArg210. Any cAsp61 residue cannot pass without being deprotonated and the proton diffusing away through the exit channel, shown in gray. (81) The energy efficiency of F_O is approximately 90% (82,83).

The mechanism has been simulated using molecular dynamics. The proton is transferred from cAsp61 (*E. coli*), whose pKa is expected to be locally reduced by electrostatic interactions with neighboring residues to promote deprotonation (84–86), to the exit half-channel, probably aided by polar residues such as E196 and intermediate water molecules (5,26,87). There are indications that the cAsp61 (or the equivalent Glu residue of other organisms) switches from a closed conformation for most of its rotational path in its membrane environment to a more open conformation as it interacts with the a-subunit and the solvation conditions therein, though the details are not entirely clear (86,88,89). The now negatively charged deprotonated cAsp61 experiences an electrostatic force toward the positively charged aArg210, bringing the deprotonated cAsp61 rapidly to the entrance channel for re-protonation (84,87,90). Intermediate states have been detected during the motion that are consistent with the 11° and 25° steps between pauses, observed in single-molecule experiments (87,91). Thus the F_O motor acts as a Brownian ratchet aided by a short-range electrostatic driving force (87,92), which maintains a high rotation rate. The conserved arginine (aArgR176 in yeast, aArg210 in *E. coli*) plays several roles crucial to the mechanism in reducing the pK_a value of the carboxylate to be deprotonated at the exit half-channel, in maintaining a strong gradient of the free energy profiles and in preventing direct transfer of protons between the entrance and exit half-channels (85). The maximum value of the torque that can be generated by F_O is

$$\tau_o = \frac{n[e\Delta\psi - k_B T(\ln 10)\Delta pH]}{2\pi}, \qquad (2)$$

where n is the number of c-subunits, ΔpH and $\Delta\psi$ are the proton gradient and membrane potential across the membrane, respectively, and e is the electronic charge (93). If $\tau_o > \tau_1$, then the F_O motor drives the F_1 motor in a clockwise direction (as viewed from the membrane), synthesizing ATP. Conversely, when $\tau_1 > \tau_o$, hydrolysis of ATP in F_1 drives the γ-stalk anticlockwise, pumping protons out of the cell.

The mismatch in rotational step-size between the F_O motor, having n values between eight and 17 for differing organisms, and the F_1 motor, having three subunits, is accommodated by elastic strain in the region of the peripheral stalk. For bacteria, the body of the single peripheral stalk has higher flexibility, whereas in mitochondria, the oligomycin sensitivity conferring protein (OSCP) domain acts as an elastic hinge (5,23,26,94). In addition to flexing in

these specific regions, the stepping mismatch between F_O and F_1 is accommodated by torsional flexing of the entire complex (5). Further, this torsional flexing applies stress to the F_1 subunits and lowers the energy of the transition state, increasing the probability of reaction (95). In contrast, the vacuolar-type *Enterococcus hirae* ATPase, EhV_OV_1, has two peripheral stalks. Here, the coupling between the V_O and V_1 subunits is more rigid, and the rotation is asymmetric and off-center, where the angular steps vary within each revolution (63,65). The differing rigidity in coupling may reflect the larger c-ring diameter of *Enterococcus hirae* of 8 nm (compared with 5 nm in *E. coli* for example) and leads to interesting stepping behavior of EhV_OV_1 (63). Another investigation of the coupling between the two motors in differing organisms indicated a broad correlation in which organisms with higher *n* values in the F_O motor are observed to have fewer dwell angles per revolution for the isolated F_1 motor (54,96). These observations point to an urgent need for more extended investigations of archaeal and vacuolar ATP synthases in order to understand the interrelationships between the number and stiffness of peripheral stalks, the nature of coupling between motors, and the number of the c-subunits. An understanding of these influences may well shed light on adaptation between organisms. There is some evidence that adaptation in ATP synthases partly reflects the bioenergetic constraints on the organism. Mitochondrial ATP synthases, which almost exclusively synthesize ATP, all have eight c-subunits, thus maximizing the ratio of ATP molecules synthesized to protons translocated. In contrast, photosynthetic organisms generally have *n* values in the range 13–15, reflecting their need to synthesize ATP under low-light conditions (low *pmf*), as well as well-lit conditions (97,98). The high *n* values may also relate to the need to avoid high values of $\Delta\psi$, which can lead to production of reactive oxygen species resulting in photodamage (97).

ATP synthesis

The ATP synthesis cycle has been studied less intensely than the hydrolysis cycle, which only requires the soluble F_1 subunit. The steps in the ATP synthesis cycle can be visualized in Fig. 2 *A*, following rotation in the clockwise direction. After release of the just-synthesized ATP molecule at $\gamma \approx 0^\circ$ where the enzyme's affinity for ATP is low, clockwise rotation driven by F_O leads to rapidly increasing affinity for P_i (34) in the region around $\gamma = 320^\circ$. Adsorption of P_i into its binding pocket electrostatically blocks ATP from binding to the catalytic site while accommodating the later binding of ADP in the range $\gamma \approx 280^\circ$–240° (52). At $\gamma \approx 320^\circ$, an additional tunnel is opened, providing an alternative access route for P_i, allowing for occasional ADP binding events before P_i binding (22). In this way, efficient ATP synthesis is possible under cellular conditions where [ATP]/[ADP] >> 1. After initial binding, both ADP and P_i then need to be tightly bound in well-defined mutual orientation as they are brought together under Coulombic repulsion (51). When the αArg376 residue is withdrawn from the catalytic site during ATP synthesis, the catalytic subunit switches from β_{DP} to β_{TP} conformation, and ATP hydrolysis becomes endergonic (23,38). On further rotation of $\gamma = 80^\circ \rightarrow 0^\circ$, the β subunit opens, and the affinity for ATP reduces rapidly (34,52). Molecular dynamics simulations provide details of the mechanism in this energetically costly step leading to release of ATP. Binding of ADP in the neighboring β_E subunit (colored blue in Fig. 2 *A*) leads to its closure, coupled through electrostatic interactions to further rotation of the γ-subunit toward $\gamma = 0^\circ$ (75,99). This rotation of the γ-stalk, also driven by the torque generated by the F_O subunit, causes distortion of the ATP binding site leading to its reduced binding affinity (99). Release of ATP from a metastable state in the region of $\gamma = 0^\circ$ leads to a flattening of the free energy profile that enables further rotation to the next catalytic state ($\gamma \approx -40^\circ$), at which a phosphate is bound at the start of the next ATP synthesis cycle (99). Thus, in the ATP synthesis cycle, binding of ADP in a neighboring subunit is energetically coupled to enable release of ATP, whereas in the ATP hydrolysis cycle, binding of ATP in a neighboring subunit drives release of ADP (75,100). The actual rotation angles at which events occur in the ATP synthesis cycle may well be shifted from those in the ATP hydrolysis cycle (23,37). Elegant single-molecule studies employing femtolitre hermetic chambers to retain synthesized ATP when rotated using magnetic tweezers in the synthesis direction confirmed the excellent chemomechanical coupling leading to at least 2.3 ATP/revolution (101).

Summary of the mechanism of F-type ATP synthase

The discussion section that follows is based on the mechanism of ATP synthase as described in sections F1 motor mechanism for ATP hydrolysis, FO motor mechanism, and ATP synthesis. In this short section, we summarize the salient main points of the mechanism to enable a general reader to engage with the discussion, referring to these previous sections for detail as necessary.

The F_1 and F_O motors generate torque in opposing directions, the greatest mean value of torque attainable being determined by Eqs. (1) and (2) respectively. F_1 generates torque primarily by progressive formation of hydrogen bonds between the catalytic site residues and the nucleotide as the β-subunit closes. This leads to a rapid increase of affinity for ATP with rotation angle in the approximate region $\gamma = 0^\circ$–60° after initial binding of ATP. Scission of the terminal phosphate is strongly endothermic until the arginine finger residue αArg376 is introduced into the catalytic site as the interface between α- and β-subunits tightens. Its introduction stabilizes the transition state, rendering the scission

reaction mildly exothermic ($\Delta G_{scission} \approx -3.3$ kJ mol^{-1}). (We refer to scission here rather than hydrolysis, to specify the rapid catalytic step alone, not including subsequent conformational changes and release of products into solution.) The F_O motor generates torque as protons are transferred from a half-channel on the low pH side of the membrane via ratcheted rotation of the c-subunits to an exit half-channel through which they are released into the cytoplasm. Unidirectionality is maintained by a positively charged Arg residue that blocks direct proton transfer between the two half-channels.

Several factors are important for the remarkably high energy efficiency of the ATP synthase. For rotation in the hydrolytic direction, the main factor is that the free energy of ATP is harnessed during binding of the nucleotide rather than during scission of ATP, which is a very rapid process occurring on the fs-ps timescale. The progressive formation of hydrogen bonds drives conformational closing of the catalytic site around the ATP molecule, which is directly coupled in turn to rotation of the central stalk. In contrast, the scission process is too rapid to contribute to rotation and hence is thermally dissipative. The binding of the nucleotide also drives conformational changes in the other β-subunits that reduce the energy dissipation of scission and reduce the binding affinity for the scission products. Scission thus produces two smaller products, ADP and Pi, which can subsequently be released from lower affinity conformations, thus resetting the cycle for adsorption of the next ATP molecule.

During ATP synthesis, Pi and ADP bind to the catalytic site and are tightly bound as they are brought together against Coulombic repulsion as the catalytic site closes, driven by the torque of the F_O motor. The most energy costly portion of the cycle is that leading to the release of ATP at $\gamma \approx 0°$, corresponding to the torque-generating region of the hydrolysis cycle. ATP release in the synthesis cycle is enabled by the energy provided by rotation of the F_O motor, together with an energy contribution from allosteric coupling to the binding of ADP in a neighboring β-subunit. In the ATP hydrolysis cycle, ADP is released using allosteric coupling to the binding of ATP in a neighboring β-subunit.

The interplay of these multiple chemical processes happening simultaneously in the three β-subunits is mediated by specific residues in the P-loop and at the noncatalytic interface between α- and β-subunits. These residues are highly conserved in the ATP synthases across the whole tree of life.

DISCUSSION

The F_1-F_O complex is a remarkable molecular machine capable of both regenerating ATP and of pumping protons or Na^+ ions energetically uphill against a concentration gradient. Its ubiquity and central role in cellular metabolism imply it arose early in life's history. The detailed understanding of the mechanism of ATP synthase, outlined above, throws light on the requirements for the functioning of both the current enzyme and its predecessors for Synthesis-First and Hydrolysis-First scenarios. Having summarized the enzyme's operation, we consider the implications of the mechanism for its origins. Efficient conversion of mechanical energy to chemical energy during ATP synthesis depends on the mechanical torque of F_O acting against the maximum counter-torque that could be generated by F_1. Its high efficiency, resulting from the direct interconversion of chemical energy and mechanical work with low dissipation as heat, is seen to be crucial as we discuss both scenarios in turn.

Implications for the ATP Synthesis-First scenario

Any model that involves the evolution of ATP synthesis before its capability for hydrolysis must, minimally, assume the existence of a membrane-bound motor that could drive a forerunner of F_1 clockwise to synthesize ATP, its generated torque exceeding the counter-torque produced by ATP hydrolysis in F_1. This forerunner of F_1 would need to be capable of adsorbing ADP and P_i and catalyze their fusion to ATP, with its affinity for the synthesized ATP being reduced sufficiently to enable its release before the next cycle could commence. Most importantly, the motor torques would need to be sufficient to generate a concentration ratio [ATP]/[ADP] high enough to maintain the primitive cell.

The physiological nucleotide concentration ratio [ATP]/[ADP] for current cells is in the range 10–1000 (47). Typical nucleotide concentrations of [ATP] = 3 mM, [ADP] = 0.4 mM, and [P_i] = 6 mM (72) give $\Delta G_{hyd} = -48$ kJ mol^{-1} (−80 pN nm in units more common at the single-molecule level). The lower limit of the [ATP]/[ADP] ratio at which cells can function for short periods is of the order of 0.1 (47,102,103). Equation 1 represents the torque generated by F_1 when operating maximally efficiently in converting the free energy of ATP hydrolysis to rotational motion. It also represents the maximum counter-torque that F_1 can generate during ATP synthesis. Efficient conversion of mechanical energy to chemical energy during ATP synthesis depends on the mechanical torque of F_O acting against the counter-torque generated by F_1. Thus, Equation 1 also limits the [ATP]/[ADP] ratio that can be attained (104,105). The F_0 motor must generate a torque greater than the torque calculated in Equation 1 to accommodate inefficient conversion or losses due to rotor rotation without a synthetic event. The relationship between the maximum attainable [ATP]/[ADP] ratio and the torque of F_1 is shown in Fig. 5 for a physiologically typical value of [P_i] of 6 mM. Applying eq. (1) with [ATP]/[ADP] = 0.1 and $\Delta G_0 = -50.6$ pN nm yields a lower limit of torque of ∼30 pN nm rad^{-1} for both F_1 and F_O: lower values of torque give [ATP]/[ADP] concentration ratios below physiological limits for current

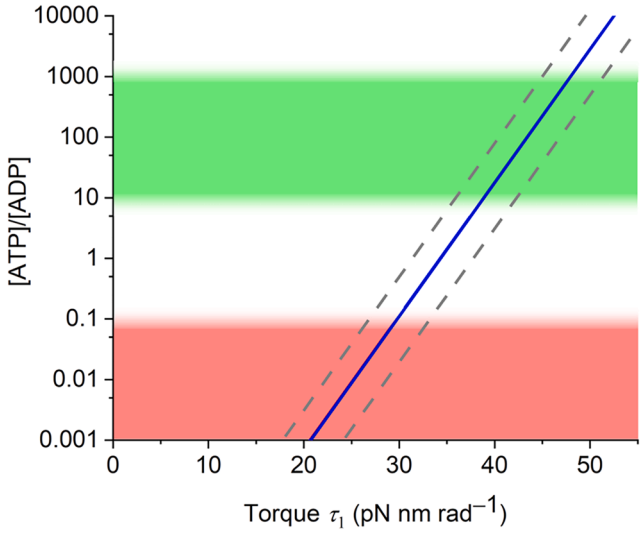

FIGURE 5 The maximum possible [ATP]/[ADP] concentration ratio that can be generated as a function of the counter-torque τ_1 of the F_1 motor for a typical phosphate concentration [Pi] of 6 mM. These are evaluated from Equation 1 with $\tau_1 = -3\Delta G_{hyd}/2\pi$. Gray dashed lines denote the corresponding ratio for approximate limiting cellular values of [Pi] = 1 mM and [Pi] = 30 mM. The green band represents the range occurring in current organisms, and the red band represents [ATP]/[ADP] ratios that are physiologically too low for bacterial cells.

Figure360▷ For a Figure360 author presentation of this figure, see https://doi.org/10.1016/j.bpj.2025.05.017.

bacteria. This lower limit of torque, $\tau_{limit} \sim 30$ pN nm rad^{-1}, is about 70% of that generated by F_1 in wild-type *Bacillus* PS3 (40–45 pN nm rad^{-1}). If it is assumed that consumption of ATP in primitive cells was less efficient than in current bacteria, then the ancient progenitor would require higher [ATP]/[ADP] ratios to offset the losses and maintain minimum concentrations during metabolism. As a result, the lower limit on the motor torques of F_1 and F_O would be correspondingly larger. This lower limit on torque of ~30 pN nm rad^{-1} for physiologically viable synthesis of ATP is consistent with experimentally measured torque values for ATP synthases from differing organisms, collated in Table 1. The measured torque values for the wild-type ATP synthases exceed this threshold, reflecting their ability to synthesize ATP at physiologically viable [ATP]/[ADP] concentration ratios. In contrast, the low measured value of torque of *Enterococcus hirae* suggests that it is incapable of maintaining physiological levels of ATP in vivo. A recent study concluded that that the physiological function of ATP synthase in *Enterococcus hirae* is limited to the specialized role of pumping Na^+ ions out of the cell, driven by ATP hydrolysis, and that it is unlikely to synthesize ATP in the organism (106).

The significance of this torque threshold and its implications for physiological viability is also seen in torque measurements on variants of the ATP synthase of *Bacillus* PS3 in which mutations have been introduced into the catalytic site by directed mutagenesis, as collated in Table 2.

TABLE 1 Measured Values of Torque for Wild-type ATP Synthases

Organism	F_1/V_1	Torque (pN.nm rad^{-1})	Reference
E. coli	F_1	63 ± 8	(107)
		56 ± 6	(108)
		50 ± 6	(109)
Bacillus PS3	F_1	43	(110)
		39 ± 4	(66)
Bos Taurus	F_1	40	(111)
Thermus thermophilus	V_1	35	(57)
		33 ± 2	(112)
Saccharomyces cerevisiae	V_1	36	(113)
Enterococcus hirae	V_1	23	(66)
		27	(66)
		22 ± 6	(114)

Substitution of single residues within the catalytic site leads to torque values below the torque threshold and hence would not be expected to viably synthesize in vivo. This prediction is confirmed by directed mutagenesis experiments on *E. coli* bacterial strains involving βE181A, βK155A or αR376A mutations, which exhibit no growth on succinate substrates, thus demonstrating loss of ATP synthesis activity (117–119). Thus, the measured values of torque for different organisms (Table 1) and for mutants of the organism *Bacillus* PS3 (Table 2) are consistent with a torque threshold of ~30 pN nm rad^{-1} for physiologically viable synthesis of ATP.

The reduction in measured torque of mutants is accompanied by a drastic reduction of rotation rate, and hence catalytic rate, by a factor of 10^3–10^5 (Table 2) (110). The increase in activation energy is likely related to the weaker binding of ATP and affects the interaction between β- and γ-subunits (39,110). For these mutated F_1 assemblies, rare fluctuations are required to attain hydrolysis of ATP, leading to much slower turnover. Conversely, the activation energy for the synthesis reaction would likely be increased requiring similarly long timescales to harness fluctuations. Increasing the number of c-subunits would favor generating higher torques at relatively low ΔpH and $\Delta\psi$. However, during most cycles, the F_O torque will drive rotation without generation of ATP, and much of the energy generated by F_O would be dissipated as heat, as observed experimentally for another mutant (116). The maximum [ATP]/[ADP] concentration ratio achievable would be substantially lower than those predicted by Equation 1, which applies to an ideally efficient ATP synthase.

Each of the above single-residue mutations within the catalytic site leads to lower attainable [ATP]/[ADP] values. If these below threshold values of torque are not physiologically feasible for current bacteria, they would have been unlikely to maintain primitive cells. Although one would not assume that early chemiosmotic complexes would involve the same sequences or structures as the current ATP synthase, these experiments do illustrate the difficulty in traversing sequence space to the contemporary complex

TABLE 2 Measured Values of Torque for ATP Synthases for *Bacillus* PS3 in which Mutations Have Been Generated within the Catalytic Site

Mutation in *Bacillus* PS3 (*E. coli* Equivalent in Brackets)	Torque (pN.nm rad^{-1})	Rotation Frequency (s^{-1})	Reference
Wild-type	43	180 ± 10	(110)
	39 ± 4	40 ± 1	(66)
	37	101 ± 50	(115)
βE190A (βE181A)	25	0.044	(110)
βK164A (βK155A)	10	0.007	(110)
αR365A (αR376A)	28	0.11	(110)
βT165S,G158A,Y341W	19	–	(116)

while maintaining physiological viability. These constraints on motor torque and energy efficiency apply generically to any ATP-based forerunner in a protocell in which ADP is converted to ATP by a rotary mechanism. Current models based on alkaline hydrothermal vents as the location for the origins of cellular life (17,120) assume very early emergence of chemiosmotic ATP synthesis. The emergence of such a system in the absence of an alternative means of generating a high [ATP]/[ADP] concentration ratio is unlikely.

Implications for the ATP Hydrolysis-First scenario

For proton pumping, driven by ATP hydrolysis in F_1, there is no threshold torque for functionality. If there had been an alternative source of ATP, maintained at an [ATP]/[ADP] ratio well away from equilibrium, then even a low torque generated by F_1 could, in principle, pump protons out of the cell to produce a small ΔpH. As the motor evolves and becomes more efficient, ΔpH would gradually increase. Initially, the Hydrolysis-First scenario seems more plausible because an early forerunner of F_1F_O-ATPase could have emerged gradually as a proton pump, and its role in chemiosmotic synthesis of ATP be a later refinement. Furthermore, recent attempts to create minimal cells that point to the first principles of life use fermentation to generate ATP and ATP synthase to maintain pH (121,122).

A viable predecessor of a F_OF_1 proton pump would minimally require a torque-generating catalytic forerunner of F_1 capable of generating rotation of a central stalk, in turn coupled to a well-defined rotor-mediated proton path through the membrane-bound early F_O involving two half-channels for inlet and outlet. Additionally, the net proton pumping rate of the ancestral F_O against the concentration gradient across the membrane would need to exceed the rate of passive proton in-diffusion to provide any benefit. Evolution of a sodium pump before a proton pump might ease this particular constraint in view of the lower permeability of Na^+ ions (123,124), and it is thought that simple fatty acids could provide sufficient resistance to proton diffusion that they comprise cell membranes while phospholipid synthesis evolves (125). However, significant proton leakage within the F_O motor, particularly at the interface between rotor and stator, would need to be avoided.

The rate of conversion of chemical energy to mechanical work is crucial for the ATP Hydrolysis-First scenario too. Not only must the F_OF_1 proton pump not dissipate most of the chemical energy to heat, but it must pump protons fast enough to maintain the pH for other cellular processes. The protein sequence of the early F_1 subunit might well differ significantly from the current one, later traversing an evolutionary pathway to the current subunit. However, mutagenesis studies illustrate the challenges in maintaining viability along such an evolutionary pathway. As noted above, single substitutions of αArg376, βLys155, or βGlu181 residues (*E. coli* equivalents) within the catalytic pocket of F_1 result in reductions in the rotation speed, and hence in catalytic rate and pumping rate, of at least three orders of magnitude (110), in addition to the adverse reduction in torque. Substitution of residues βThr156, βArg182, βGlu185, βMet209, βAsp242 or βArg246 in the catalytic site are similarly detrimental (51,126,127) as are those of the residues αPro281, αAla285, αArg296, αGlu299, αArg303, αAla306 and αArg376 in the interfacial region of the α-subunit involved in the loosening and tightening of the interface with the β-subunit (126). In the F_O subunit, substitution of aArg210 aGly218, aGlu219 or aHis245 severely affects function (128). In such directed mutagenesis studies, simultaneous mutations at a neighboring site can sometimes restore function. For example, mutation of aArg210 in the a-subunit of F_O leads to complete loss of activity, yet a double mutation in which aArg210 is switched with aGlu252 (i.e., aR210E and aE252R mutations) is capable of both ATP synthesis and ATP-driven proton translocation (129). To date, no such compensating pairs of mutations have been found around the catalytic site of F_1-ATPase: hydrolysis rates are severely impaired in each case regardless of mutations elsewhere. These mutagenesis studies sample a miniscule fraction of protein sequence space, yet their slow pumping rates limit the cell complexity that could be maintained and severely constrain the later stages of evolutionary pathways to the current ATP synthase.

The ATP Hydrolysis-First scenario additionally requires a preexisting alternative source of ATP on the early earth that maintained a concentration ratio [ATP]/[ADP] > 0.1 for physiological viability. Published models for this scenario (13,130,131) suggest that ATP was initially supplied by fermentation. These models unsurprisingly do not provide

a means to satisfy the above constraints as they largely predate the structural details of F_1 (31) and the understanding of its mechanism. Several factors show that fermentation is not a viable primitive forerunner of chemiosmosis but rather appeared later (17). Any proposed Hydrolysis-First scenario that predates the ATP synthase and fermentation would require a viable biotic or abiotic means of generating ATP. Despite the early popularity of the ATP Hydrolysis-First scenario, the scenarios presented to date have not survived closer scrutiny, and new ideas are required for this mechanism to be plausible.

Co-option of earlier forerunners of F_O and F_1

In view of the central role of the catalytic site of F_1 in cellular life, we need to consider in more detail possible co-option of an ancient functioning ATPase with an ion channel in an ancestral complex. Sequence and structural similarities between F_1 and hexameric helicases have long been noted (132–134). These similarities suggest the attractive possibility that an ATP-driven helicase, as a forerunner of F_1, might have been co-opted with an ion channel, as a forerunner of the membrane-bound F_O, in an ancestral ATP synthase (124,135). Mulkidjanian et al. propose a model in which an ion channel in a membrane might have bound a RNA strand translocated through a RNA helicase, the complex evolving via an intermediate RNA translocase into a protein translocase (135). There are several difficulties with such a pathway that arise directly from the mechanism of ATP synthase. Despite its superficial similarity with F_O, a single ion channel oriented normal to the plane of the membrane clearly cannot be coupled to drive rotational motion of F_1 as a result of its symmetry. The interface between rotor and stator (currently the a/c subunit interface) is needed to maintain impermeability to protons. If these conditions for impermeability were not met, F_O could not pump protons, and F_1 would have wastefully consumed ATP for no benefit during rotation, dissipating chemical energy as heat.

A related difficulty for the co-option of a functioning ATPase and an ion channel involves the nontrivial coupling of the two complexes. An uncoupled F_O motor would dissipate any proton gradient across the membrane, and an uncoupled F_1-like motor would likewise dissipate ATP, causing such a protocell to drift rapidly toward equilibrium. Such dissipation of free energy is guarded against in current cellular life both during assembly of the F_1F_O-ATP synthase complex and during its operation. Assembly of the ATP synthase complex proceeds in bacteria in a specific sequence to prevent such dissipation: the $\alpha_3\beta_3\gamma\varepsilon$, the membrane-bound c_n-ring and the ab_2 stator complex firstly form as three entities. The δ-subunit, aided by interactions at the a-c interface, then locks these three together, only forming the proton pathway at the a-c interface when ATP synthesis and proton pumping functions of the full complex are enabled (136,137). Likewise, wasteful hydrolysis of ATP is prevented by regulation of rotation in the hydrolytic direction of the central stalk. Photosynthetic organisms display a wide range of regulatory mechanisms to suppress ATP hydrolysis in the dark, involving redox switches on the γ-subunit, interactions of the ε-subunit with β- and γ-subunits and protein inhibitors (98,138,139). Likewise, bacteria such as *Bacillus* PS3 employ conformational changes in the ε-subunit to inhibit rotation in the hydrolysis direction when the ATP concentration is low while enabling rotation in the synthesis direction (101,140–142), though details of the ε-subunit interactions can differ between bacterial species (143). During any transitional pathway to the fully formed F_O-F_1 complex, early evolution of rudimentary mechanisms that performed these protective functions of inhibiting the dissipation of the proton gradient and ATP would have been vital.

In addition to the above difficulties arising from the mechanism, the supposed co-option of an ion channel and a helicase requires a primitive helicase to predate the ATP synthase. This is unlikely on phylogenetic considerations: hexameric helicases in bacteria and archaea are based on different protein folds (bacterial based on the RecA fold, archaeal on the AAA+ fold), and they translocate ssDNA in different directions (bacterial on the lagging strand, archaeal on the leading strand, in common with eukaryotes) (144). If one assumes that features that are shared between bacteria and archaea predate those that differ, the ATP synthase enzyme would be considered to have originated earlier than helicases and to have featured in the LUCA (17,145). Thus, evolution of ATP synthase by co-option of helicases and ion channels seems unrealistic on phylogenetic and mechanistic grounds. Maybe advances in sequencing and metagenomics analysis will uncover hitherto unknown prospective progenitors of ATP synthase, but they too will be required to meet the functional requirements during co-option described herein.

SUMMARY AND OUTLOOK

The ATP synthase complex comprises the membrane-bound F_O motor coupled to the F_1 motor by a common stalk. The F_O motor effectively operates as a Brownian ratchet translocating protons across the membrane. The F_1 ATPase generates a counter-torque by hydrolysis of ATP. Its mechanism is now largely understood in terms of the physics, chemistry, as well as biochemistry as a result of incremental and occasionally dramatic developments in experimental and computational approaches. Nanoscale single-molecule experiments of increasing complexity have been crucial here. Improvements in time resolution and numerical analysis of data, e.g., Ref. (146), will further improve capabilities and be applied to other cellular processes and systems. Structural studies originally dependent on x-ray crystallography, limited to static time-averaged systems that crystallize, have been revolutionized by developments in cryo-EM,

enabling dynamic processes to be sampled. Molecular dynamics simulations of full rotation cycles of ATP synthase are limited by the size of the system and the timescales of conformational changes and rotation. One beneficial future direction should be the generation of free energy landscapes that cover the full rotation cycle of F_1 and the coupled F_OF_1 ATP synthase, which is computationally less demanding than the dynamics of the full cycle. A second future direction should be extensive experimental and computational studies on archaeal and vacuolar ATP synthases to understand more fully the similarities and differences between these and the better-understood F-type complexes. When the understanding of similarities and differences between archaeal and bacterial ATP synthases has clarified and matured, this will naturally lead into a further future research direction in working through their implications for earlier evolutionary pathways.

This coupled motor mechanism of ATP synthase along with the motor torque having extreme sensitivity to changes in sequence constrains models for the origin of this enzyme. Any forerunner, in either the Hydrolysis-First or Synthesis-First scenarios, minimally depends on a functioning catalytic site in which either synthesis or hydrolysis of ATP occurred at viable rates. The F_O subunit depends on its proton half-channels, directionality of the rotational path maintained by electrostatic blocking, and its impermeability to protons at the rotor-stator interface. Since protons take the path of least resistance across the membrane, any primitive membrane would have needed to be relatively impervious to protons. An early forerunner of the F_O-F_1 complex would also have needed a means of coupling the rotation of the two subunits with a central stalk as well as mechanochemical coupling of binding energy changes in F_1 to drive rotation or to synthesize ATP. Free-standing, uncoupled, F_O and F_1 subunits would detrimentally dissipate the free energy maintained by the proton gradient and the [ATP]/[ADP] ratio respectively.

In order to generate a physiologically viable [ATP]/[ADP] ratio of greater than 0.1, both F_O and F_1 motors need to exceed a threshold of $\sim$30 pN nm rad^{-1}. This torque threshold would also apply to the enzyme's forerunners that employed rotational catalysis. Indeed, since it is likely that a primeval forerunner was less efficient in exploiting the free energy for ATP hydrolysis, the constraints on the [ATP]/[ADP] ratio generated by chemiosmosis, and hence on the motor torques, would have been even more demanding. These constraints appear to be prohibitive for the ATP Synthesis-First models of the origin of life, including those that locate early life at hydrothermal vents, requiring a very early origin of chemiosmosis (17,147).

The alternative ATP Hydrolysis-First scenario, while not needing to fulfill this torque threshold, involves further constraints to avoid thermal dissipation of free energy in a viscous environment. Firstly, since energy released during bond scission cannot drive much slower conformational changes, ATP hydrolysis within the catalytic site of a forerunner of F_1 needed to maintain the products ADP and P_i in tight proximity so that the reactant and product energies of the scission substep are much closer together than in solution. As a consequence, the binding energy for ATP in another subunit is harnessed to drive the rotation of the subunit binding the reaction products until it reaches a low affinity confirmation and releases ADP and P_i. Secondly, the proton pumping rate would need to exceed the passive proton diffusion rate into the cell. Single mutations in the F_1 catalytic site result in a reduction of the pumping rate by three to five orders of magnitude (110), limiting the possible proton diffusion rate through the membrane and motor assembly itself. Thirdly, a means for coordinating the hydrolysis event and the sequence of binding events would have been essential to generate torque. In current ATP synthase, this role is provided by allosteric interactions in the $(\alpha\beta)_3$ hexamer, including the modulated interactions of the aArg376 residue with the catalytic site, and the interactions between β and γ subunits. Fourthly, the ATP Hydrolysis-First scenario would have required an alternative source of ATP on the early earth that maintained the [ATP]/[ADP] concentration ratio well away from equilibrium. Fermentation is not likely to have fulfilled this role in view of evidence that it followed rather than preceded chemiosmosis (17). Published models that propose an early proton pump driven by ATP hydrolysis (13,130,131) do not fulfill these constraints.

Neither ATP Synthesis-First nor the ATP Hydrolysis-First scenarios appear to be consistent with the constraints arising directly from the detailed mechanism of ATP synthase. It is hardly surprising that published proposals for the origin of chemiosmosis have proved unsatisfactory as they largely predate the detailed understanding of the workings of the enzyme. Whereas the catalytic site and the catalytic process are very similar in all ATP synthases, there are clear variations between organisms arising from adaptation. For example, F-type, A-type, and V-type ATP synthases have differing numbers and rigidity of peripheral stalks (24). As discussed above, the number of c-subunits in the F_O motor varies between eight and 17 for differing organisms and can be broadly related to bioenergetic function (97,98), evidencing adaptation to the organism's environmental requirements. Likewise, the regulatory interactions between the central stalk and the α/β hexamer that inhibit wasteful hydrolysis of ATP also vary between organisms (143). However, the constraints that arise from the mechanism of ATP synthase on both the Synthesis-First and Hydrolysis-First scenarios require new ideas for continuous pathways in the origin of chemiosmosis, where an understanding of the relationship between archaeal and bacterial ATP synthases might be significant. A particular challenge is to propose a workable means of coupling the ancestral equivalents of F_O and F_1 while avoiding rapid dissipation of either proton gradient or ATP concentration, leading to equilibration. The constraints outlined here are useful for evaluating both published models for the origin of chemiosmosis and those proposed in the future.

ACKNOWLEDGMENTS

Work at the Molecular Foundry was supported by the Office of Science, Office of Basic Energy Sciences, of the U.S. Department of Energy under Contract No. DE-AC02-05CH11231. The authors are thankful to Prof. Ryota Iino for helpful suggestions.

DECLARATION OF INTERESTS

The authors declare no competing interests.

SUPPORTING MATERIAL

Supporting material can be found online at https://doi.org/10.1016/j.bpj.2025.05.017.

REFERENCES

1. Hulett, H. R. 1970. Non-enzymatic hydrolysis of adenosine phosphates. *Nature.* 225:1248–1249. https://doi.org/10.1038/2251248a0.
2. Wang, C., W. Huang, and J.-L. Liao. 2015. QM/MM Investigation of ATP Hydrolysis in Aqueous Solution. *J. Phys. Chem. B.* 119:3720–3726. https://doi.org/10.1021/jp512960e.
3. Kühlbrandt, W. 2019. Structure and Mechanisms of F-Type ATP Synthases. *Annu. Rev. Biochem.* 88:515–549. https://doi.org/10.1146/annurev-biochem-013118-110903.
4. Noji, H., H. Ueno, and D. G. G. McMillan. 2017. Catalytic robustness and torque generation of the F_1-ATPase. *Biophys. Rev.* 9:103–118. https://doi.org/10.1007/s12551-017-0262-x.
5. Sobti, M., J. L. Walshe, …, A. G. Stewart. 2020. Cryo-EM structures provide insight into how E. coli F_1F_O ATP synthase accommodates symmetry mismatch. *Nat. Commun.* 11:2615. https://doi.org/10.1038/s41467-020-16387-2.
6. Noji, H., and H. Ueno. 2022. How Does F_1-ATPase Generate Torque?: Analysis From Cryo-Electron Microscopy and Rotational Catalysis of Thermophilic F_1. *Front. Microbiol.* 13:904084. https://doi.org/10.3389/fmicb.2022.904084.
7. Sobti, M., Y. C. Zeng, …, A. G. Stewart. 2023. Changes within the central stalk of E. coli F_1F_O-ATP synthase observed after addition of ATP. *Commun. Biol.* 6:26. https://doi.org/10.1038/s42003-023-04414-z.
8. Watanabe, R., K. V. Tabata, …, H. Noji. 2013. Biased Brownian stepping rotation of FoF1-ATP synthase driven by proton motive force. *Nat. Commun.* 4:1631. https://doi.org/10.1038/ncomms2631.
9. Adachi, K., K. Oiwa, …, K. Kinosita. 2007. Coupling of Rotation and Catalysis in F_1-ATPase Revealed by Single-Molecule Imaging and Manipulation. *Cell.* 130:309–321. https://doi.org/10.1016/j.cell.2007.05.020.
10. Astumian, R. D. 2019. Kinetic asymmetry allows macromolecular catalysts to drive an information ratchet. *Nat. Commun.* 10:3837. https://doi.org/10.1038/s41467-019-11402-7.
11. Branscomb, E., T. Biancalani, …, M. Russell. 2017. Escapement mechanisms and the conversion of disequilibria; the engines of creation. *Phys. Rep.* 677:1–60. https://doi.org/10.1016/j.physrep.2017.02.001.
12. Astumian, R. D. 2007. Design principles for Brownian molecular machines: how to swim in molasses and walk in a hurricane. *Phys. Chem. Chem. Phys.* 9:5067–5083. https://doi.org/10.1039/b708995c.
13. Raven, J. A., and F. A. Smith. 1976. The evolution of chemiosmotic energy coupling. *J. Theor. Biol.* 57:301–312. https://doi.org/10.1016/0022-5193(76)90003-5.
14. Broda, E. 1975. The Evolution of the Bioenergetic Processes. Kent. Elsevier Science.
15. Clarke, P. H., and S. R. Elsden. 1980. The earliest catabolic pathways. *J. Mol. Evol.* 15:333–338. https://doi.org/10.1007/BF01733139.
16. Alberts, B. 2002. Molecular Biology of the Cell, 4th ed. Garland Science, New York.
17. Lane, N., J. F. Allen, and W. Martin. 2010. How did LUCA make a living? Chemiosmosis in the origin of life. *Bioessays.* 32:271–280. https://doi.org/10.1002/bies.200900131.
18. Mahendrarajah, T. A., E. R. R. Moody, …, A. Spang. 2023. ATP synthase evolution on a cross-braced dated tree of life. *Nat. Commun.* 14:7456. https://doi.org/10.1038/s41467-023-42924-w.
19. Lane, N., and W. F. Martin. 2012. The Origin of Membrane Bioenergetics. *Cell.* 151:1406–1416. https://doi.org/10.1016/j.cell.2012.11.050.
20. Martin, W., and M. J. Russell. 2007. On the origin of biochemistry at an alkaline hydrothermal vent. *Phil. Trans. R. Soc. B.* 362:1887–1925. https://doi.org/10.1098/rstb.2006.1881.
21. Barge, L. M., and R. E. Price. 2022. Diverse geochemical conditions for prebiotic chemistry in shallow-sea alkaline hydrothermal vents. *Nat. Geosci.* 15:976–981. https://doi.org/10.1038/s41561-022-01067-1.
22. Sobti, M., H. Ueno, …, A. G. Stewart. 2021. The six steps of the complete F_1-ATPase rotary catalytic cycle. *Nat. Commun.* 12:4690. https://doi.org/10.1038/s41467-021-25029-0.
23. Murphy, B. J., N. Klusch, …, W. Kühlbrandt. 2019. Rotary substates of mitochondrial ATP synthase reveal the basis of flexible F_1-F_O coupling. *Science.* 364:eaaw9128. https://doi.org/10.1126/science.aaw9128.
24. Courbon, G. M., and J. L. Rubinstein. 2022. CryoEM Reveals the Complexity and Diversity of ATP Synthases. *Front. Microbiol.* 13:864006. https://doi.org/10.3389/fmicb.2022.864006.
25. Pinke, G., L. Zhou, and L. A. Sazanov. 2020. Cryo-EM structure of the entire mammalian F-type ATP synthase. *Nat. Struct. Mol. Biol.* 27:1077–1085. https://doi.org/10.1038/s41594-020-0503-8.
26. Spikes, T. E., M. G. Montgomery, and J. E. Walker. 2020. Structure of the dimeric ATP synthase from bovine mitochondria. *Proc. Natl. Acad. Sci. USA.* 117:23519–23526. https://doi.org/10.1073/pnas.2013998117.
27. Sharma, S., M. Luo, …, M. Liao. 2024. Conformational ensemble of yeast ATP synthase at low pH reveals unique intermediates and plasticity in F1–Fo coupling. *Nat. Struct. Mol. Biol.* 31:657–666. https://doi.org/10.1038/s41594-024-01219-4.
28. Morowitz, H. J. 1992. Beginnings of Cellular Life: Metabolism Recapitulates Biogenesis. Yale University Press, New Haven.
29. Boyer, P. D. 1993. The binding change mechanism for ATP synthase — Some probabilities and possibilities. *Biochim. Biophys. Acta.* 1140:215–250. https://doi.org/10.1016/0005-2728(93)90063-L.
30. Boyer, P. D. 1989. A perspective of the binding change mechanism for ATP synthesis. *FASEB J.* 3:2164–2178. https://doi.org/10.1096/fasebj.3.10.2526771.
31. Abrahams, J. P., A. G. Leslie, …, J. E. Walker. 1994. Structure at 2.8 Å resolution of F_1-ATPase from bovine heart mitochondria. *Nature.* 370:621–628. https://doi.org/10.1038/370621a0.
32. Bowler, M. W., M. G. Montgomery, …, J. E. Walker. 2007. Ground state structure of F_1-ATPase from bovine heart mitochondria at 1.9 Å resolution. *J. Biol. Chem.* 282:14238–14242. https://doi.org/10.1074/jbc.M700203200.
33. Noji, H., R. Yasuda, …, K. Kinosita. 1997. Direct observation of the rotation of F_1-ATPase. *Nature.* 386:299–302. https://doi.org/10.1038/386299a0.
34. Watanabe, R., D. Okuno, …, H. Noji. 2011. Mechanical modulation of catalytic power on F_1-ATPase. *Nat. Chem. Biol.* 8:86–92. https://doi.org/10.1038/nchembio.715.
35. Martin, J. L., R. Ishmukhametov, …, W. D. Frasch. 2014. Anatomy of F_1-ATPase powered rotation. *Proc. Natl. Acad. Sci. USA.* 111:3715–3720. https://doi.org/10.1073/pnas.1317784111.
36. Saita, E. i., T. Suzuki, …, M. Yoshida. 2015. Simple mechanism whereby the F_1-ATPase motor rotates with near-perfect chemomechanical energy conversion. *Proc. Natl. Acad. Sci. USA.* 112:9626–9631. https://doi.org/10.1073/pnas.1422885112.

37. Toyabe, S., T. Watanabe-Nakayama, …, E. Muneyuki. 2011. Thermodynamic efficiency and mechanochemical coupling of F_1-ATPase. *Proc. Natl. Acad. Sci. USA.* 108:17951–17956. https://doi.org/10.1073/pnas.1106787108.

38. Dittrich, M., S. Hayashi, and K. Schulten. 2004. ATP hydrolysis in the β_{TP} and β_{DP} catalytic sites of F_1-ATPase. *Biophys. J.* 87:2954–2967. https://doi.org/10.1529/biophysj.104.046128.

39. Hayashi, S., H. Ueno, …, H. Noji. 2012. Molecular mechanism of ATP hydrolysis in F_1-ATPase revealed by molecular simulations and single-molecule observations. *J. Am. Chem. Soc.* 134:8447–8454. https://doi.org/10.1021/ja211027m.

40. Mukherjee, S., and A. Warshel. 2011. Electrostatic origin of the mechanochemical rotary mechanism and the catalytic dwell of F_1-ATPase. *Proc. Natl. Acad. Sci. USA.* 108:20550–20555. https://doi.org/10.1073/pnas.1117024108.

41. Klusch, N., B. J. Murphy, …, W. Kühlbrandt. 2017. Structural basis of proton translocation and force generation in mitochondrial ATP synthase. *eLife.* 6:e33274. https://doi.org/10.7554/eLife.33274.

42. Kiani, F. A., and S. Fischer. 2016. Comparing the catalytic strategy of ATP hydrolysis in biomolecular motors. *Phys. Chem. Chem. Phys.* 18:20219–20233. https://doi.org/10.1039/C6CP01364C.

43. Bowler, M. W., M. J. Cliff, …, G. M. Blackburn. 2010. Why did Nature select phosphate for its dominant roles in biology? *New J. Chem.* 34:784. https://doi.org/10.1039/b9nj00718k.

44. Komoriya, Y., T. Ariga, …, H. Noji. 2012. Principal role of the arginine finger in rotary catalysis of F_1-ATPase. *J. Biol. Chem.* 287:15134–15142. https://doi.org/10.1074/jbc.M111.328153.

45. Kobayashi, R., H. Ueno, …, H. Noji. 2020. Rotary catalysis of bovine mitochondrial F_1-ATPase studied by single-molecule experiments. *Proc. Natl. Acad. Sci. USA.* 117:1447–1456. https://doi.org/10.1073/pnas.1909407117.

46. Blankenship, R. E. 2009. Molecular Mechanisms of Photosynthesis, 4. Blackwell Science.

47. Meyrat, A., and C. von Ballmoos. 2019. ATP synthesis at physiological nucleotide concentrations. *Sci. Rep.* 9:3070. https://doi.org/10.1038/s41598-019-38564-0.

48. Arai, H. C., A. Yukawa, …, H. Noji. 2014. Torque generation mechanism of F_1-ATPase upon NTP binding. *Biophys. J.* 107:156–164. https://doi.org/10.1016/j.bpj.2014.05.016.

49. Okazaki, K. i., and S. Takada. 2011. Structural comparison of F_1-ATPase: interplay among enzyme structures, catalysis, and rotations. *Structure.* 19:588–598. https://doi.org/10.1016/j.str.2011.01.013.

50. Sugawa, M., K.-I. Okazaki, …, T. Nishizaka. 2016. F_1-ATPase conformational cycle from simultaneous single-molecule FRET and rotation measurements. *Proc. Natl. Acad. Sci. USA.* 113:E2916–E2924. https://doi.org/10.1073/pnas.1524720113.

51. Senior, A. E., S. Nadanaciva, and J. Weber. 2002. The molecular mechanism of ATP synthesis by F_1F_O-ATP synthase. *Biochim. Biophys. Acta.* 1553:188–211. https://doi.org/10.1016/s0005-2728(02)00185-8.

52. Adachi, K., K. Oiwa, …, K. Kinosita. 2012. Controlled rotation of the F_1-ATPase reveals differential and continuous binding changes for ATP synthesis. *Nat. Commun.* 3:1022. https://doi.org/10.1038/ncomms2026.

53. Suzuki, T., K. Tanaka, …, M. Yoshida. 2014. Chemomechanical coupling of human mitochondrial F_1-ATPase motor. *Nat. Chem. Biol.* 10:930–936. https://doi.org/10.1038/nchembio.1635.

54. Zarco-Zavala, M., R. Watanabe, …, H. Noji. 2020. The $3 \times 120^\circ$ rotary mechanism of *Paracoccus denitrificans* F_1-ATPase is different from that of the bacterial and mitochondrial F_1-ATPases. *Proc. Natl. Acad. Sci. USA.* 117:29647–29657. https://doi.org/10.1073/pnas.2003163117.

55. Furuike, S., M. Nakano, …, K. Yokoyama. 2011. Resolving stepping rotation in Thermus thermophilus H+-ATPase/synthase with an essentially drag-free probe. *Nat. Commun.* 2:233. https://doi.org/10.1038/ncomms1215.

56. Minagawa, Y., H. Ueno, …, R. Iino. 2013. Basic Properties of Rotary Dynamics of the Molecular Motor Enterococcus hirae V_1-ATPase. *J. Biol. Chem.* 288:32700–32707. https://doi.org/10.1074/jbc.M113.506329.

57. Imamura, H., M. Takeda, …, K. Yokoyama. 2005. Rotation scheme of V_1-motor is different from that of F_1-motor. *Proc. Natl. Acad. Sci. USA.* 102:17929–17933. https://doi.org/10.1073/pnas.0507764102.

58. Forgac, M. 2007. Vacuolar ATPases: rotary proton pumps in physiology and pathophysiology. *Nat. Rev. Mol. Cell Biol.* 8:917–929. https://doi.org/10.1038/nrm2272.

59. Grüber, G., M. S. S. Manimekalai, …, V. Müller. 2014. ATP synthases from archaea: The beauty of a molecular motor. *Biochimica et Biophysica Acta - Bioenergetics.* 1837:940–952. https://doi.org/10.1016/j.bbabio.2014.03.004.

60. Iida, T., Y. Minagawa, …, R. Iino. 2019. Single-molecule analysis reveals rotational substeps and chemo-mechanical coupling scheme of Enterococcus hirae V_1-ATPase. *J. Biol. Chem.* 294:17017–17030. https://doi.org/10.1074/jbc.RA119.008947.

61. Abbas, Y. M., D. Wu, …, J. L. Rubinstein. 2020. Structure of V-ATPase from the mammalian brain. *Science.* 367:1240–1246. https://doi.org/10.1126/science.aaz2924.

62. Zhou, L., and L. A. Sazanov. 2019. Structure and conformational plasticity of the intact Thermus thermophilus V/A-type ATPase. *Science.* 365:eaaw9144. https://doi.org/10.1126/science.aaw9144.

63. Otomo, A., T. Iida, …, R. Iino. 2022. Direct observation of stepping rotation of V-ATPase reveals rigid component in coupling between V_o and V_1 motors. *Proc. Natl. Acad. Sci. USA.* 119:e2210204119. https://doi.org/10.1073/pnas.2210204119.

64. Kishikawa, J., A. Nakanishi, …, K. Yokoyama. 2022. Structural snapshots of V/A-ATPase reveal the rotary catalytic mechanism of rotary ATPases. *Nat. Commun.* 13:1213. https://doi.org/10.1038/s41467-022-28832-5.

65. Burton-Smith, R. N., C. Song, …, K. Murata. 2023. Six states of Enterococcus hirae V-type ATPase reveals non-uniform rotor rotation during turnover. *Commun. Biol.* 6:755. https://doi.org/10.1038/s42003-023-05110-8.

66. Ueno, H., Y. Minagawa, …, R. Iino. 2014. Torque Generation of Enterococcus hirae V-ATPase. *J. Biol. Chem.* 289:31212–31223. https://doi.org/10.1074/jbc.M114.598177.

67. Sielaff, H., J. Martin, …, W. D. Frasch. 2016. Power Stroke Angular Velocity Profiles of Archaeal A-ATP Synthase Versus Thermophilic and Mesophilic F-ATP Synthase Molecular Motors. *J. Biol. Chem.* 291:25351–25363. https://doi.org/10.1074/jbc.M116.745240.

68. Kinosita, K., K. Adachi, and H. Itoh. 2004. Rotation of F_1-ATPase: How an ATP-Driven Molecular Machine May Work. *Annu. Rev. Biophys. Biomol. Struct.* 33:245–268. https://doi.org/10.1146/annurev.biophys.33.110502.132716.

69. Li, C.-B., and S. Toyabe. 2020. Efficiencies of molecular motors: a comprehensible overview. *Biophys. Rev.* 12:419–423. https://doi.org/10.1007/s12551-020-00672-x.

70. Leighton, M. P., and D. A. Sivak. 2023. Inferring Subsystem Efficiencies in Bipartite Molecular Machines. *Phys. Rev. Lett.* 130:178401. https://doi.org/10.1103/PhysRevLett.130.178401.

71. Dittrich, M., and K. Schulten. 2005. Zooming in on ATP hydrolysis in F_1. *J. Bioenerg. Biomembr.* 37:441–444. https://doi.org/10.1007/s10863-005-9487-7.

72. Nam, K., and M. Karplus. 2019. Insights into the origin of the high energy-conversion efficiency of F_1-ATPase. *Proc. Natl. Acad. Sci. USA.* 116:15924–15929. https://doi.org/10.1073/pnas.1906816116.

73. Masaike, T., N. Mitome, …, M. Yoshida. 2000. Rotation of F_1-ATPase and the hinge residues of the beta subunit. *J. Exp. Biol.* 203:1–8. https://doi.org/10.1242/jeb.203.1.1.

74. Gao, Y. Q., W. Yang, …, M. Karplus. 2003. A model for the cooperative free energy transduction and kinetics of ATP hydrolysis by F_1-ATPase. *Proc. Natl. Acad. Sci. USA.* 100:11339–11344. https://doi.org/10.1073/pnas.1334188100.

75. Czub, J., M. Wieczór, …, H. Grubmüller. 2017. Mechanochemical Energy Transduction during the Main Rotary Step in the Synthesis Cycle of F_1-ATPase. *J. Am. Chem. Soc.* 139:4025–4034. https://doi.org/10.1021/jacs.6b11708.

76. Czub, J., and H. Grubmüller. 2014. Rotation Triggers Nucleotide-Independent Conformational Transition of the Empty β Subunit of F_1 -ATPase. *J. Am. Chem. Soc.* 136:6960–6968. https://doi.org/10.1021/ja500120m.

77. Bai, C., M. Asadi, and A. Warshel. 2020. The catalytic dwell in ATPases is not crucial for movement against applied torque. *Nat. Chem.* 12:1187–1192. https://doi.org/10.1038/s41557-020-0549-6.

78. Junge, W., H. Lill, and S. Engelbrecht. 1997. ATP synthase: an electrochemical transducer with rotatory mechanics. *Trends Biochem. Sci.* 22:420–423. https://doi.org/10.1016/s0968-0004(97)01129-8.

79. Vik, S. B., and B. J. Antonio. 1994. A mechanism of proton translocation by F_1F_O-ATP synthases suggested by double mutants of the a subunit. *J. Biol. Chem.* 269:30364–30369. https://doi.org/10.1016/S0021-9258(18)43822-7.

80. Hahn, A., J. Vonck, …, W. Kühlbrandt. 2018. Structure, mechanism, and regulation of the chloroplast ATP synthase. *Science.* 360: eaat4318. https://doi.org/10.1126/science.aat4318.

81. Ho, B. K., and F. Gruswitz. 2008. HOLLOW: generating accurate representations of channel and interior surfaces in molecular structures. *BMC Struct. Biol.* 8:49. https://doi.org/10.1186/1472-6807-8-49.

82. Silverstein, T. P. 2014. An exploration of how the thermodynamic efficiency of bioenergetic membrane systems varies with c-subunit stoichiometry of F_1F_O-ATP synthases. *J. Bioenerg. Biomembr.* 46:229–241. https://doi.org/10.1007/s10863-014-9547-y.

83. Kubo, S., T. Niina, and S. Takada. 2020. Molecular dynamics simulation of proton-transfer coupled rotations in ATP synthase F_O motor. *Sci. Rep.* 10:8225. https://doi.org/10.1038/s41598-020-65004-1.

84. Kamiyama, Y., D. Parkin, and M. Takano. 2023. Torque generation mechanism in F_O motor of ATP synthase elucidated by free-energy and Coulomb-energy landscapes along the c-ring rotation. *Biochem. Biophys. Res. Commun.* 651:56–61. https://doi.org/10.1016/j.bbrc.2023.01.085.

85. Marciniak, A., P. Chodnicki, …, J. Czub. 2022. Determinants of Directionality and Efficiency of the ATP Synthase F_o Motor at Atomic Resolution. *J. Phys. Chem. Lett.* 13:387–392. https://doi.org/10.1021/acs.jpclett.1c03358.

86. Srivastava, A. P., M. Luo, …, D. M. Mueller. 2018. High-resolution cryo-EM analysis of the yeast ATP synthase in a lipid membrane. *Science.* 360:eaas9699. https://doi.org/10.1126/science.aas9699.

87. Blanc, F. E. C., and G. Hummer. 2024. Mechanism of proton-powered c-ring rotation in a mitochondrial ATP synthase. *Proc. Natl. Acad. Sci. USA.* 121:e2314199121. https://doi.org/10.1073/pnas.2314199121.

88. Symersky, J., V. Pagadala, …, D. M. Mueller. 2012. Structure of the c10 ring of the yeast mitochondrial ATP synthase in the open conformation. *Nat. Struct. Mol. Biol.* 19:485-91–S1. https://doi.org/10.1038/nsmb.2284.

89. Pogoryelov, D., Ö. Yildiz, …, T. Meier. 2009. High-resolution structure of the rotor ring of a proton-dependent ATP synthase. *Nat. Struct. Mol. Biol.* 16:1068–1073. https://doi.org/10.1038/nsmb.1678.

90. Parkin, D., and M. Takano. 2023. Coulombic Organization in Membrane-Embedded Rotary Motor of ATP Synthase. *J. Phys. Chem. B.* 127:1552–1562. https://doi.org/10.1021/acs.jpcb.2c07875.

91. Yanagisawa, S., and W. D. Frasch. 2021. pH-dependent 11° F_1F_O-ATP synthase sub-steps reveal insight into the F_O torque generating mechanism. *eLife.* 10:e70016. https://doi.org/10.7554/eLife.70016.

92. Hwang, W., and M. Karplus. 2019. Structural basis for power stroke vs. Brownian ratchet mechanisms of motor proteins. *Proc. Natl. Acad. Sci. USA.* 116:19777–19785. https://doi.org/10.1073/pnas.1818589116.

93. Nicholls, D. G., and S. J. Ferguson. 2013. Bioenergetics, Fourth edition. Academic Press, Elsevier, Amsterdam.

94. Guo, H., and J. L. Rubinstein. 2022. Structure of ATP synthase under strain during catalysis. *Nat. Commun.* 13:2232. https://doi.org/10.1038/s41467-022-29893-2.

95. Friddle, R. W. 2008. Unified Model of Dynamic Forced Barrier Crossing in Single Molecules. *Phys. Rev. Lett.* 100:138302. https://doi.org/10.1103/PhysRevLett.100.138302.

96. Noji, H., H. Ueno, and R. Kobayashi. 2020. Correlation between the numbers of rotation steps in the ATPase and proton-conducting domains of F- and V-ATPases. *Biophys. Rev.* 12:303–307. https://doi.org/10.1007/s12551-020-00668-7.

97. Davis, G. A., and D. M. Kramer. 2020. Optimization of ATP Synthase c–Rings for Oxygenic Photosynthesis. *Front. Plant Sci.* 10:1778. https://doi.org/10.3389/fpls.2019.01778.

98. Cheuk, A., and T. Meier. 2021. Rotor subunits adaptations in ATP synthases from photosynthetic organisms. *Biochem. Soc. Trans.* 49:541–550. https://doi.org/10.1042/BST20190936.

99. Badocha, M., M. Wieczór, …, J. Czub. 2023. Molecular mechanism and energetics of coupling between substrate binding and product release in the F_1 -ATPase catalytic cycle. *Proc. Natl. Acad. Sci. USA.* 120:e2215650120. https://doi.org/10.1073/pnas.2215650120.

100. Antes, I., D. Chandler, …, G. Oster. 2003. The unbinding of ATP from F_1-ATPase. *Biophys. J.* 85:695–706. https://doi.org/10.1016/S0006-3495(03)74513-5.

101. Rondelez, Y., G. Tresset, …, H. Noji. 2005. Highly coupled ATP synthesis by F1-ATPase single molecules. *Nature.* 433:773–777. https://doi.org/10.1038/nature03277.

102. Jung, S.-R., Y. Deng, …, D.-S. Koh. 2018. Minimizing ATP depletion by oxygen scavengers for single-molecule fluorescence imaging in live cells. *Proc. Natl. Acad. Sci. USA.* 115:E5706–E5715. https://doi.org/10.1073/pnas.1717724115.

103. Rohwer, J. M., P. R. Jensen, …, H. V. Westerhoff. 1996. Changes in the cellular energy state affect the activity of the bacterial phosphotransferase system. *Eur. J. Biochem.* 235:225–230. https://doi.org/10.1111/j.1432-1033.1996.00225.x.

104. Chiwata, R., A. Kohori, …, K. Kinosita. 2014. None of the Rotor Residues of F_1-ATPase Are Essential for Torque Generation. *Biophys. J.* 106:2166–2174. https://doi.org/10.1016/j.bpj.2014.04.013.

105. Usukura, E., T. Suzuki, …, M. Yoshida. 2012. Torque generation and utilization in motor enzyme F_OF_1-ATP synthase: half-torque F_1 with short-sized pushrod helix and reduced ATP Synthesis by half-torque F_OF_1. *J. Biol. Chem.* 287:1884–1891. https://doi.org/10.1074/jbc.M111.305938.

106. Otomo, A., L. G. Hui Zhu, …, R. Iino. 2025. ATP synthesis of Enterococcus hirae V-ATPase driven by sodium motive force. *J. Biol. Chem.* 301:108422. https://doi.org/10.1016/j.jbc.2025.108422.

107. Hornung, T., R. Ishmukhametov, …, W. D. Frasch. 2008. Determination of torque generation from the power stroke of Escherichia coli F_1-ATPase. *Biochim. Biophys. Acta.* 1777:579–582. https://doi.org/10.1016/j.bbabio.2008.04.016.

108. Junge, W., H. Sielaff, and S. Engelbrecht. 2009. Torque generation and elastic power transmission in the rotary FOF1-ATPase. *Nature.* 459:364–370. https://doi.org/10.1038/nature08145.

109. Pänke, O., D. A. Cherepanov, …, W. Junge. 2001. Viscoelastic Dynamics of Actin Filaments Coupled to Rotary F-ATPase: Angular Torque Profile of the Enzyme. *Biophys. J.* 81:1220–1233. https://doi.org/10.1016/S0006-3495(01)75780-3.

110. Watanabe, R., Y. Matsukage, …, H. Noji. 2014. Robustness of the Rotary Catalysis Mechanism of F_1-ATPase. *J. Biol. Chem.* 289:19331–19340. https://doi.org/10.1074/jbc.M114.569905.

111. Kobayashi, R., H. Ueno, …, H. Noji. 2023. Molecular mechanism on forcible ejection of ATPase inhibitory factor 1 from mitochondrial ATP synthase. *Nat. Commun.* 14:1682. https://doi.org/10.1038/s41467-023-37182-9.

112. Hayashi, K., H. Ueno, …, H. Noji. 2010. Fluctuation Theorem Applied to F 1 -ATPase. *Phys. Rev. Lett.* 104:218103. https://doi.org/10.1103/PhysRevLett.104.218103.

113. Hirata, T., A. Iwamoto-Kihara, …, M. Futai. 2003. Subunit Rotation of Vacuolar-type Proton Pumping ATPase. *J. Biol. Chem.* 278:23714–23719. https://doi.org/10.1074/jbc.M302756200.

114. Otomo, A., J. Wiemann, …, R. Iino. 2024. Visualizing Single V-ATPase Rotation Using Janus Nanoparticles. *Nano Lett.* 24: 15638–15644. https://doi.org/10.1021/acs.nanolett.4c04109.

115. Yukawa, A., R. Iino, …, H. Noji. 2015. Key Chemical Factors of Arginine Finger Catalysis of F_1 -ATPase Clarified by an Unnatural Amino Acid Mutation. *Biochemistry.* 54:472–480. https://doi.org/10.1021/bi501138b.

116. Toyabe, S., and E. Muneyuki. 2015. Single molecule thermodynamics of ATP synthesis by F_1 -ATPase. *New J. Phys.* 17:015008. https://doi.org/10.1088/1367-2630/17/1/015008.

117. Futai, M., M. Park, …, M. Maeda. 1994. Catalysis and energy coupling of H+-ATPase (ATP synthase): Molecular biological approaches. *Biochim. Biophys. Acta.* 1187:165–170. https://doi.org/10.1016/0005-2728(94)90104-X.

118. Zhao, C., H. Syed, …, Z. Ahmad. 2016. Functional importance of αIle-346 and αIle-348 in the catalytic sites of Escherichia coli ATP synthase. *Arch. Biochem. Biophys.* 592:27–37. https://doi.org/10.1016/j.abb.2016.01.009.

119. Nadanaciva, S., J. Weber, …, A. E. Senior. 1999. Importance of F_1 -ATPase Residue α-Arg-376 for Catalytic Transition State Stabilization. *Biochemistry.* 38:15493–15499. https://doi.org/10.1021/bi9917683.

120. Barge, L. M., I. J. Doloboff, …, I. Kanik. 2014. Pyrophosphate synthesis in iron mineral films and membranes simulating prebiotic submarine hydrothermal precipitates. *Geochem. Cosmochim. Acta.* 128:1–12. https://doi.org/10.1016/j.gca.2013.12.006.

121. Hutchison, C. A., R.-Y. Chuang, …, J. C. Venter. 2016. Design and synthesis of a minimal bacterial genome. *Science.* 351:aad6253. https://doi.org/10.1126/science.aad6253.

122. Pelletier, J. F., L. Sun, …, E. A. Strychalski. 2021. Genetic requirements for cell division in a genomically minimal cell. *Cell.* 184:2430–2440.e16. https://doi.org/10.1016/j.cell.2021.03.008.

123. Mulkidjanian, A. Y., M. Y. Galperin, …, E. V. Koonin. 2008. Evolutionary primacy of sodium bioenergetics. *Biol. Direct.* 3:13. https://doi.org/10.1186/1745-6150-3-13.

124. Nirody, J. A., I. Budin, and P. Rangamani. 2020. ATP synthase: Evolution, energetics, and membrane interactions. *J. Gen. Physiol.* 152: e201912475. https://doi.org/10.1085/jgp.201912475.

125. Yu, F., J. Fei, …, J. Li. 2025. Chemiosmotic ATP synthesis by minimal protocells. *Cell Rep. Phys. Sci.* 6:102461. https://doi.org/10.1016/j.xcrp.2025.102461.

126. Futai, M., H. Omote, …, Y. Wada. 2000. Synthase (H^+-ATPase): coupling between catalysis, mechanical work, and proton translocation. *Biochim. Biophys. Acta.* 1458:276–288. https://doi.org/10.1016/s0005-2728(00)00080-3.

127. Ahmad, Z., F. Okafor, and T. F. Laughlin. 2011. Role of Charged Residues in the Catalytic Sites of *Escherichia coli* ATP Synthase. *J. Amino Acids.* 2011:785741. https://doi.org/10.4061/2011/785741.

128. von Ballmoos, C., A. Wiedenmann, and P. Dimroth. 2009. Essentials for ATP synthesis by F_1F_O ATP synthases. *Annu. Rev. Biochem.* 78:649–672. https://doi.org/10.1146/annurev.biochem.78.081307.104803.

129. Ishmukhametov, R. R., J. B. Pond, …, S. B. Vik. 2008. ATP synthesis without R210 of subunit a in the Escherichia coli ATP synthase. *Biochim. Biophys. Acta.* 1777:32–38. https://doi.org/10.1016/j.bbabio.2007.11.004.

130. Cross, R. L., and V. Müller. 2004. The evolution of A-F-and V-type ATP synthases and ATPases: reversals in function and changes in the H^+/ATP coupling ratio. *FEBS Lett.* 576:1–4. https://doi.org/10.1016/j.febslet.2004.08.065.

131. Nelson, N., and L. Taiz. 1989. The evolution of H^+-ATPases. *Trends Biochem. Sci.* 14:113–116. https://doi.org/10.1016/0968-0004(89)90134-5.

132. Gomis-Rüth, F. X., G. Moncalián, …, M. Coll. 2001. The bacterial conjugation protein TrwB resembles ring helicases and F_1-ATPase. *Nature.* 409:637–641. https://doi.org/10.1038/35054586.

133. Walker, J. E. 1998. ATP Synthesis by Rotary Catalysis (Nobel lecture). *Angew. Chem. Int. Ed. Engl.* 37:2308–2319. https://doi.org/10.1002/(SICI)1521-3773(19980918)37:17<2308::AID-ANIE2308>3.0.CO;2-W.

134. Walker, J. E., and A. L. Cozens. 1986. Evolution of ATP synthase. *Chem. Scripta.* 26B:263–272.

135. Mulkidjanian, A. Y., K. S. Makarova, …, E. V. Koonin. 2007. Inventing the dynamo machine: the evolution of the F-type and V-type ATPases. *Nat. Rev. Microbiol.* 5:892–899. https://doi.org/10.1038/nrmicro1767.

136. Rühle, T., and D. Leister. 2015. Assembly of F_1F_O-ATP synthases. *Biochim. Biophys. Acta.* 1847:849–860. https://doi.org/10.1016/j.bbabio.2015.02.005.

137. Vu Huu, K., R. Zangl, …, N. Morgner. 2022. Bacterial F-type ATP synthases follow a well-choreographed assembly pathway. *Nat. Commun.* 13:1218. https://doi.org/10.1038/s41467-022-28828-1.

138. Yi, S., X. Guo, …, X. Lu. 2024. Structure, Regulation, and Significance of Cyanobacterial and Chloroplast Adenosine Triphosphate Synthase in the Adaptability of Oxygenic Photosynthetic Organisms. *Microorganisms.* 12:940. https://doi.org/10.3390/microorganisms12050940.

139. Feniouk, B. A., and M. Yoshida. 2008. Regulatory mechanisms of proton-translocating F_OF_1-ATP Synthase. *In* Bioenergetics. H. S. Penefsky and G. Schäfer, eds Springer Berlin Heidelberg, Berlin, Heidelberg. https://doi.org/10.1007/400_2007_043.

140. Yagi, H., N. Kajiwara, …, H. Akutsu. 2007. Structures of the thermophilic F_1-ATPase epsilon subunit suggesting ATP-regulated arm motion of its C-terminal domain in F_1. *Proc. Natl. Acad. Sci. USA.* 104:11233–11238. https://doi.org/10.1073/pnas.0701045104.

141. Guo, H., T. Suzuki, and J. L. Rubinstein. 2019. Structure of a bacterial ATP synthase. *eLife.* 8:e43128. https://doi.org/10.7554/eLife.43128.

142. Iino, R., R. Hasegawa, …, H. Noji. 2009. Mechanism of Inhibition by C-terminal α-Helices of the ϵ Subunit of Escherichia coli FoF_1-ATP Synthase. *J. Biol. Chem.* 284:17457–17464. https://doi.org/10.1074/jbc.M109.003798.

143. Sielaff, H., T. M. Duncan, and M. Börsch. 2018. The regulatory subunit ε in Escherichia coli F_OF_1-ATP synthase. *Biochim. Biophys. Acta. Bioenerg.* 1859:775–788. https://doi.org/10.1016/j.bbabio.2018.06.013.

144. O'Donnell, M. E., and H. Li. 2018. The ring-shaped hexameric helicases that function at DNA replication forks. *Nat. Struct. Mol. Biol.* 25:122–130. https://doi.org/10.1038/s41594-018-0024-x.

145. Weiss, M. C., S. Neukirchen, …, F. L. Sousa. 2016. Reply to 'Is LUCA a thermophilic progenote?'. *Nat. Microbiol.* 1:16230. https://doi.org/10.1038/nmicrobiol.2016.230.

146. Volkán-Kacsó, S., L. Q. Le, …, R. A. Marcus. 2019. Method to extract multiple states in F_1 -ATPase rotation experiments from jump distributions. *Proc. Natl. Acad. Sci. USA.* 116:25456–25461. https://doi.org/10.1073/pnas.1915314116.

147. Russell, M. J., and A. J. Hall. 1997. The emergence of life from iron monosulphide bubbles at a submarine hydrothermal redox and pH front. *J. Geol. Soc. London.* 154:377–402. https://doi.org/10.1144/gsjgs.154.3.0377.